Transition metal dichalcogenide-based functional membrane: Synthesis, modification, and water purification applications

Huarong Peng, Renheng Wang, Liang Mei, Qingyong Zhang, Ting Ying, Zhengfang Qian, Amir Barati Farimani, Damien Voiry, Zhiyuan Zeng

HAL Id: hal-04055653

https://hal.umontpellier.fr/hal-04055653

Submitted on 3 Oct 2023

Transition metal dichalcogenide-based functional membrane: Synthesis, modification, and water purification applications

Huarong Peng,[1] Renheng Wang,[1,*] Liang Mei,[2] Qingyong Zhang,[2] Ting Ying,[2] Zhengfang Qian,[1,*] Amir Barati Farimani,[3] Damien Voiry,[4,*] and Zhiyuan Zeng[2,*]

SUMMARY

Transition metal dichalcogenide (TMDC) nanomaterials have become excellent candidates for next-generation functional membranes. In the past few years, tremendous encouraging experimental and theoretical studies have been conducted on TMDC-based nanomaterials, which opened up a new direction for developing highly selective and permeable membranes. Herein, we systematically summarize the recent advances in 2D TMDC nanomaterials and their application in water purification. The physical and chemical properties of TMDC-based functional membranes that facilitate water purification are stated in detail. Simultaneously, the theoretical investigations used to understand the desalination process of the TMDC-based membranes are also summarized. Furthermore, we sum up the synthesis method and discuss the modification strategies for TMDC-based membrane in water purification application. Finally, the challenges and perspectives on the future development of TMDC-based functional membrane for water purification, as well as the future research direction for functionalization of TMDC-based membrane, are proposed.

INTRODUCTION

Drinking water scarcity, caused by worldwide industrialization and population growth, is one of the most critical issues for modern society.[1,2] Based on the report of the World Health Organization, more than eight hundred million people on earth are short of basic water services and nearly four billion people live in a severe water scarcity conditions at least 1 month each year.[3] The even worse situation that we human beings face today is that freshwater resources are being polluted and are deteriorating. There are increasing amounts of contaminants caused by industrial or agricultural activity entering into our water supply. These contaminants include toxic heavy metal ions, organic matter, industrial chemicals, micropollutants (such as endocrine disruptors, pesticides, and personal care products), which seriously risk human health. To alleviate the shortage of drinkable water and insufficient fresh water supply, it is important to develop advanced water purification techniques to accomplish water recycling from seawater, brackish groundwater, and wastewater.

Three promising water purification technologies have been established to generate drinkable water based on their energy supply: solar thermal desalination (STD), capacitive deionization (CDI), and reverse osmosis (RO). Solar-driven STD techniques provide high-quality pure water at a low rate using renewable solar energy.[4,5] Electrically driven CDI techniques are usually applied for the selective removal of trace amounts of target

PROGRESS AND POTENTIAL

Exploring highly efficient water purification technology to alleviate the shortage of drinkable water is vital in addressing the global water crisis. Among various strategies, a reverse osmosis technique using transition metal dichalcogenide (TMDC)-based membranes has gained increasing attention owing to their promising desalination performance and eco-friendliness. However, there is no comprehensive review to summarize recent progress on TMDC-based membranes so far. This review gives a systematical overview from history, synthesis routes, modification strategies, and the underlying mechanism for TMDC-based membranes. Furthermore, challenges and perspectives for future development of TMDC-based membranes are also stated, which can benefit researchers to better understand the desalination process of TMDC-based membranes, and also inspire scientists entering into this exciting field.

contaminants, such as Ca^{2+}, Mg^{2+}, SO_4^{2-}, Pb^{2+}, CrO_4^{2-}, UO_2^{2+}, and Br^-, by regulating ion adsorption on the electrode interface or intercalation in the bulk electrode.[6,7] Compared with STD and CDI, the pressure-driven RO technique is an effective and environmentally friendly method for water purification and desalination; however, the main challenge of the RO process is the development of highly efficient and low-cost separation membranes.[8,9] The main purpose of membrane construction is to design and fabricate suitable semipermeable membranes, which only permit water molecules to penetrate while leaving salt ions unpassed. However, commercialized thin-film composite polymeric membranes promote the advancement of the RO technique; the water permeability is approximately <0.24 L per square meter per day per MPa due to the selectivity-permeability trade-off when satisfying the demand of high salt rejection.[10] In addition, the selectivity and stability of this membrane are not optimal, and low fouling and chlorine resistance of the polymeric membranes restricted further improvements of the RO process for water purification and desalination.[11]

To improve the separation efficiency of RO, exploring highly selective and permeable two-dimensional (2D) membrane materials with high fouling and chlorine resistance is the main goal for next-generation desalination membranes. Among all the 2D membrane materials, graphene oxide (GO) has been intensively studied for water desalination and micropollutant removal.[12–15] The superior performance of GO membranes is attributed to the balance between the hydrophobic and hydrophilic regions of the GO nanosheets, atomic thickness, large slip length, high mechanical robustness (elastic modulus: ∼110–420 GPa),[16] and antimicrobial properties.[17] However, the hydrophilic oxygenated functional groups of GO nanosheets cause uncontrollable swelling behavior of the membrane in solution, which increases their porosity, thus influencing the sieving performance in the form of selectivity and water permeance.[18] Similar to GO, MXene-based membranes exhibit good properties for water purification.[14,19] However, they also experience membrane swelling behavior in aqueous media, leading to deteriorating performance in ion and molecule rejection.[20] Hence, efforts are required to control the swelling behavior of GO- and MXene-based membranes to enhance their sieving performance.

Transition metal dichalcogenide (TMDC) has been extensively investigated as a next-generation functional membrane material owing to its unique physical and chemical properties. As shown in Figure 1A, monolayer MX_2 exhibits a sandwich structure consisting of one layer of transition metal atoms (M = Mo, W, V, Nb, Ta, Ti, or Zr) between two layers of chalcogen atoms (X = S, Se, or Te). Each MX_2 monolayer stacks together by van der Waals forces to form TMDC bulk materials. The two most common TMDC polymorphs are usually found in nature: the distorted tetragonal phase (1T) with an octahedral coordination and hexagonal phase (2H) with a trigonal prismatic coordination. The advantages of TMDCs are as follows (1) layered TMDC nanosheet membranes can remain stable without swelling issues in aqueous solution over a wide pH range because of the strong van der Waals force existing in TMDC sheets.[21,22] (2) Owing to the stacking of three atomic layers in the sequence of chalcogen-metal-chalcogen, single-layer TMDCs exhibit higher mechanical strength than single-layer GO.[23,24] (3) The relatively low water affinity of TMDC nanosheets ensures the formation of rapid water molecular nanochannels.[25,26] (4) The single-layer structure of TMDCs is prone to construct pores for fast water permeation,[27,28] which is accomplished by digging holes into TMDCs nanosheets (Figure 1B). (5) The surface layer of chalcogen atoms is easy to functionalize[29,30] and, after functionalization, the interlayer spacing (Figure 1C) can be expanded, thus facilitating water molecules to transport through. (6) TMDCs nanosheets exhibit high antibacterial activity with no toxicity, thereby making them beneficial to water treatment.[31,32]

[1]Key Laboratory of Optoelectronic Devices and Systems of Ministry of Education and Guangdong Province, College of Physics and Optoelectronic Engineering, Shenzhen University, Shenzhen 518060, P. R. China

[2]Department of Materials Science and Engineering, City University of Hong Kong, 83 Tat Chee Avenue, Kowloon, Hong Kong 999077, P. R. China

[3]Department of Mechanical Engineering, Carnegie Mellon University, Pittsburgh, PA 15213, USA

[4]Institut Européen des Membranes, IEM, UMR 5635, Université Montpellier, ENSCM, CNRS, Montpellier, France

*Correspondence: wangrh@szu.edu.cn (R.W.), zq001@szu.edu.cn (Z.Q.), damien.voiry@umontpellier.fr (D.V.), zhiyzeng@cityu.edu.hk (Z.Z.)
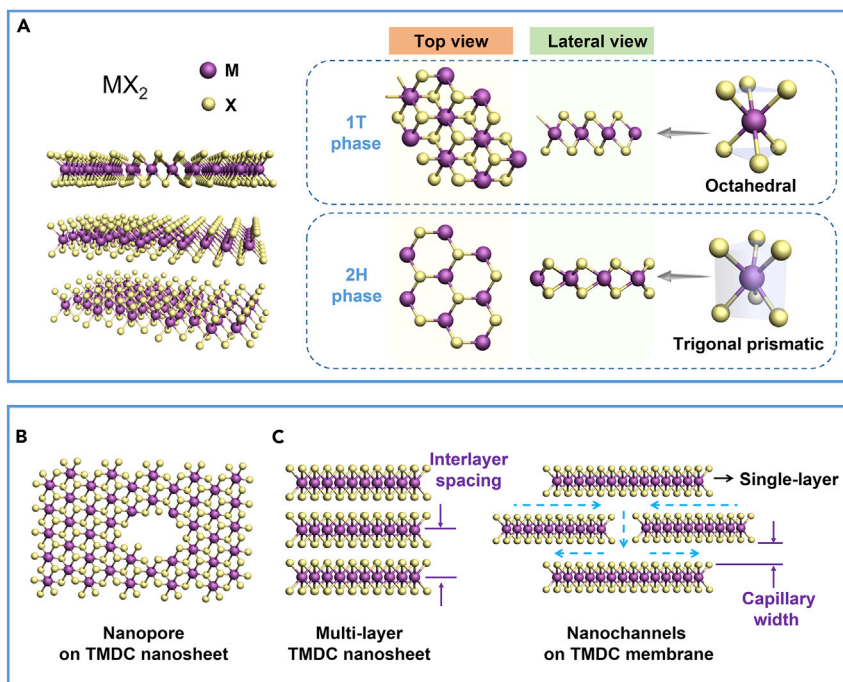
Figure 1. Structure models of TMDC nanomaterials

(A) Schematic illustration of the TMDC structure showing the stacking of three atomic layers in the sequence of chalcogen-metal-chalcogen (MX_2: M represents metal atom, X represents chalcogen atom). Top and lateral views of 1T (up) and 2H (down) phases for TMDC monolayer. The octahedral coordination for the metal atom in 1T phase and trigonal prismatic coordination for the metal atom in 2H phase are also shown.

(B) Schematic illustration of the derived pore of TMDC in top view.

(C) Schematic illustration of interlayer spacing, nanochannels, and capillary width in TMDCs.

To date, several reviews have focused on the 2D nanomaterial-based separation membranes (e.g., GO[33,34] and MXenes[35,36]) used for water purification and desalination. Although one review on TMDC-based membranes mentioned water purification,[37] there is no comprehensive review on TMDC-based membranes mainly focusing on water purification with basic principles, formation mechanism, features, and properties included. Therefore, a review including the above aspects is highly needed for readers to understand TMDC-based membranes used in water purification, which is beneficial for the future development of membrane. In this review, we summarize the recent experimental and theoretical research progress on 2D TMDC functional membrane materials (e.g., MoS_2, WS_2, and TiS_2) and their application in the area of water purification (Figure 2).

First, we introduce the basic knowledge of water purification, including its principle, classification, performance evaluation criteria, and influencing factors for performance. Second, the controllable synthesis of 2D layered TMDC materials for membrane engineering processes is introduced. Third, the functionalization approaches for TMDC functional materials used for membrane manufacturing are discussed. Fourth, theoretical investigations of TMDC membranes are summarized, which will facilitate an understanding of the mechanism of the sieving process. Finally, the challenges and opportunities for the development of TMDC-based functional membranes are discussed. This review may be able to guide the rational design and fabrication of high-efficiency TMDC-based membranes for water purification and inspire the broad interest of other scientists in this field.
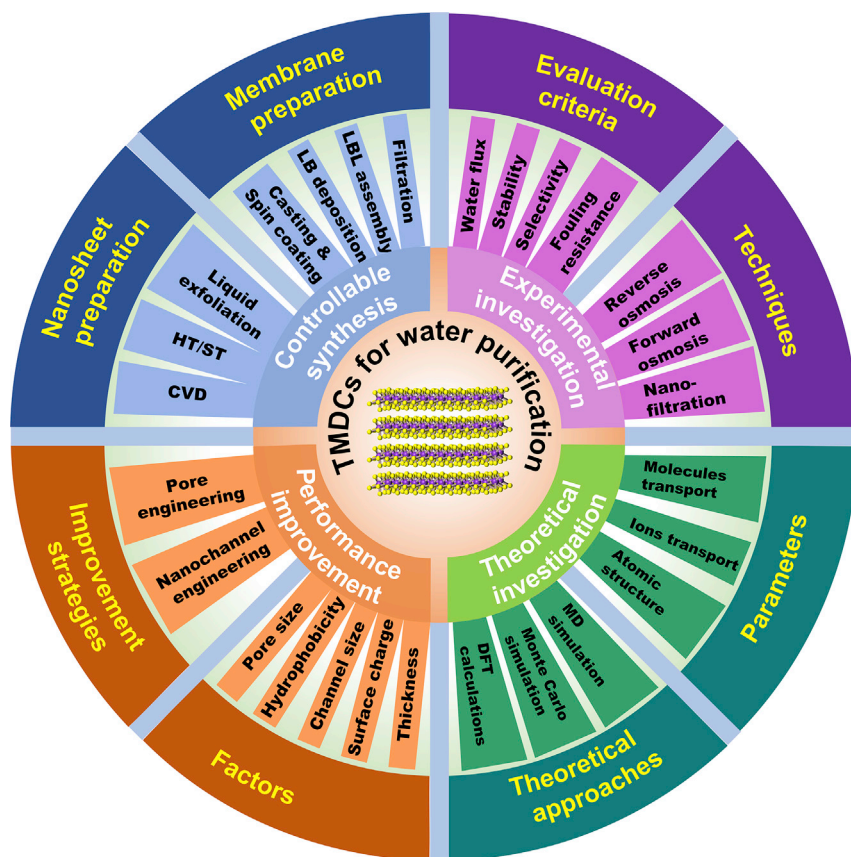
Figure 2. Content of the review on 2D TMDC-based membrane for water purification

UNDERSTANDING WATER DESALINATION

Classification of water desalination technologies

Based on water desalination classification, membrane-based filtration technology comprises microfiltration, ultrafiltration, nanofiltration, and RO. As shown in Figure 3A, microfiltration membranes, with a cutoff limit of 100–10,000 nm, are typically used to filter suspended solids, bacteria, and microorganisms that are larger than viruses and protozoa. The pore size of ultrafiltration membranes is two orders of magnitude smaller than that of microfiltration membranes (i.e., 10–100 nm), which can be used to remove viruses, algal toxins, and some natural organic matter. Nanofiltration membranes have small and narrow pore size ranges (1–10 nm), which remove most heavy metal ions, dyes, and other small organic matter for water softening applications. The above three techniques are fully developed, and the used commercial polymeric membranes exhibit considerable separation performance. Some researchers summarized the recent advances in nanomaterials applied in these techniques and provided outlook and prospective studies.[38–40] However, the quality of the obtained filtered water could not reach the standard of drinkable water according to the World Health Organization.

RO is a leading and reliable technology with high impurity rejection efficiency, which is applied in industrial and domestic applications. As a state-of-the-art membrane separation technology, RO produces ultrapure water by completely removing all dissolved salts, colloids, inorganic molecules, and macromolecular organics (molecular weight >100). At present, commercial semipermeable membranes applied in
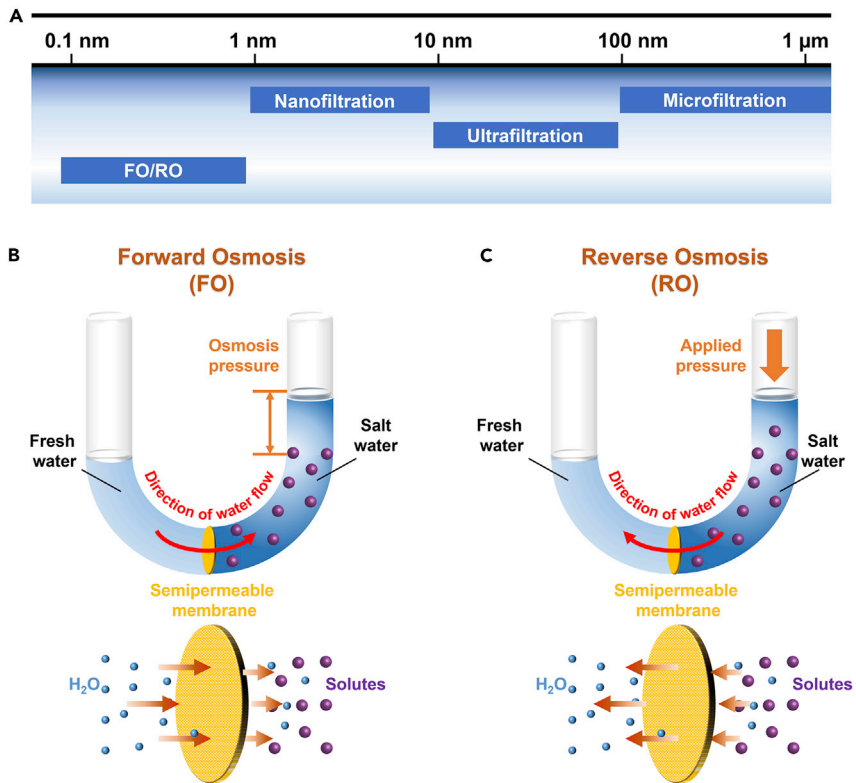
Figure 3. Membrane-based techniques and their desalination principles
(A) Schematic illustration of the membrane-based technique. The principle of (B) forward osmosis and (C) reverse osmosis for desalination and water purification.

RO are polyamide (PA) and cellulose acetate thin films, offering a cutoff limit of 0.1–1 nm.[41,42] To date, the yield of pure water and the mechanical robustness of RO membranes need to be improved when developing an energy-efficient and environmentally friendly desalination technology. In addition, the pressure applied in the lower concentration liquid in RO leads to huge energy consumption, thus greatly increasing the cost of desalination. Therefore, improving ion rejection, reusability, and lowering energy consumption in RO is currently the main challenge faced by all scientific researchers and producers.

Principle of water desalination

The principle of water desalination is to remove various types of undesired species and obtain potable freshwater from the abundant seawater resources on earth. The driving force for the separation process is either the natural osmotic pressure or hydrostatic pressure.

The focus of membrane-based filtration processes is to design novel 2D nanoporous separation membranes with strong ion rejection and large water flux. These separation membranes have thicknesses ranging from several nanometers to several hundred micrometers when acting as a semipermeable barrier block. As shown in Figure 3B, for forward osmosis (FO), water molecules penetrate the semipermeable membranes from a low-concentration solution (e.g., fresh water) to a higher-concentration solution (e.g., salt water) under a condition of osmotic pressure difference.[43,44] Conversely, unlike FO, which relies on osmotic pressure caused by concentration difference, RO works under an additional applied pressure of a few

to dozens of bars (Figure 3C).[45,46] When additional pressure is applied to the saline feed stream until the hydrostatic pressure exceeds the osmotic pressure, water molecules transit from the pressurized feed stream to the pure permeate stream through the semipermeable membrane. Thus, high-quality ultrapure water can be collected. As the focus of this review, RO technology involves the blocking of target ions and/or molecules through the 2D TMDC nanomaterials-based separation membrane based on the sieving mechanism.

Performance evaluation criteria

To understand the situation and challenges of RO desalination, we need to clarify the evaluation criteria. Some critical parameters need to be addressed when fabricating efficient semipermeable membranes, such as water flux (i.e., water permeance), selectivity, stability, and fouling resistance.

Water flux (i.e., water permeance)

Water flux is a quantitative criterion for the performance evaluation of membrane-based desalination techniques. It is defined as the volume of permeable water generated per area of applied pressure per time ($L\ m^{-2}\ h^{-1}\ bar^{-1}$, i.e., LMH/bar). The water permeance of the designed semipermeable membrane should be equal to or even surpass that of existing commercial membranes. Hydrostatic pressure, temperature, and salt ion concentration on the feed side are three main factors that affect the water flux of the membrane. The spacing, thickness, and water affinity also affect the water flux.

Selectivity

Selectivity reflects the ability of the membrane to reject ions and molecules dissolved in the feed side solution from penetrating. At present, the target components of membrane rejection are mineral salt ions, heavy metal ions, dye molecules, and micropollutants. Among them, the effective rejection of small salt ions, such as Li^+, Na^+, K^+, Ca^{2+}, Mg^{2+}, Cl^-, and SO_4^{2-}, has been proven difficult for developing semipermeable membranes. Generally, salt rejection is the percentage of removed cations and anions, as described in Equation 1:[47]

$$R = \left(1 - \frac{C_1}{C_0}\right) \times 100\%, \qquad \text{(Equation 1)}$$

where R is the salt rejection, C_1 is the detected salt ion concentration in the permeate water, and C_0 is the detected salt ion concentration in the feed water.

Stability

Stability is another metric used to assess the performance of semipermeable membranes. Because these membranes need to be immersed in pending processed liquids with a broad pH range under high hydraulic pressure, they must provide a considerable mechanical and chemical stability to resist water flow and corrosion. Inducing suitable pre-treatment processes on the membrane surface is essential to ensure its long-term operational stability under harsh operating conditions.[48] The working time or recycled number of membranes are usually determined to evaluate their stability.

Fouling resistance

Fouling resistance is an important parameter for semipermeable membranes, which relates to the stability of the membrane. When contaminants (e.g., macromolecular organic compounds, dissolved inorganic substances, and oil droplets) deposit on the membrane surface and block pores/channels of the membrane, fouling

occurs, which results in substantially reduced permeability. The fouling resistance is closely related to the chemistry, roughness, and charge of membrane surface. First, surface modification (e.g., coating a thin film or grafting some polymer chains on the membrane surface) is an effective strategy to mitigate membrane fouling problems. This is because coating or grafting materials do not have affinity toward the foulants, thus avoiding any interactions between foulants and membranes. Second, reducing membranes' surface roughness could prevent foulants depositing on membrane surfaces. Third, increasing membranes' surface charge could also stop counter-charged foulants depositing on membrane surfaces, thus improving the antifouling performance of the membrane. Zou and co-workers demonstrated that coating MoS_2 on a thin film composite nanofiltration membrane improved its fouling resistance to bovine serum albumin due to the weaker MoS_2-foulant interactive forces, the negatively charged surface, and the reduced surface roughness of 2D MoS_2 nanoplatelets.[49] Membranes constructed using those materials with unique anti-chlorine and antibacterial properties could prevent the growth of bacteria, thereby extending the lifetime of membranes, while limiting the formation of undesirable biofilms. Therefore, the prevention of fouling is a critical parameter for developing advanced membranes.

Influencing factors

The factors that influence the water purification and desalination performance of a semipermeable membrane are their chemical and physical properties, such as pore size, interlayer spacing, hydrophobicity, and surface charge. In addition, the thickness of the membrane also influences their performance.

Pore size

A suitable pore size is a key factor in ensuring the performance of membrane-based water desalination.[50] Typically, pores in the TMDCs layers are artificially formed during the synthesis process (e.g., probe-type sonication[51]) or subsequent treatments (e.g., oxygen plasma etching process,[12] electrochemical reaction for pore fabrication,[52] transmission electron microscopy [TEM]-drilled technique[53,54]). Based on the steric resistance effect of the sieving mechanism, the pore size of a semipermeable membrane largely determines the size of target penetrating molecules, ions, and substances. A simple comparison of this factor could result in a rough assessment of the TMDC-based membrane. The varied size of the nanopores in TMDCs benefits the separation of impurities and pollutants in unclean water. The control of the pore size is currently an active field of research but the effective methods to generate pores have been limited so far.

Interlayer spacing

For 2D layered nanomaterials, interlayer spacing is a key parameter that forms channels.[55] When permeants penetrate membranes through the nanoconfined channels, they transform from the bulk state to nanofluids after absorbing energy. The energy required depends on the channel size (e.g., capillary width), which limits the entry of fluids. Thus, interlayer spacing influences the water transport pathway. By grafting functional groups or intercalation molecules/ions, researchers have demonstrated the modulation of the interlayer spacing of TMDC-based functional membranes to a certain extent. For example, Zeng's group grafted ethanol and amide functional groups on MoS_2 structures to expand the interlayer spacing of MoS_2-based membranes, which improved the water permeation performance with good rejection rate.[56]

Hydrophobicity

The hydrophobic and hydrophilic nature of the separation membrane is determined by the polarity of the surface molecules. It is difficult to transport hydrated ions during the separation process. Meanwhile, increasing the hydrophobic property could enhance the antifouling property of the membranes. This is because hydrophilic contaminants rarely adhere to or deposit on hydrophobic surfaces.

Surface charge

The surface properties of TMDC membranes directly affect the penetration of water molecules and the adsorption of charged ions in the matrix. Modified semipermeable membranes with surface charge could enhance their antifouling properties owing to electrostatic repulsion effect. The negative charged TMDC membrane could prevent positively charged contaminants to adhere on membrane surface.

Thickness

The permeation decreases exponentially with membrane thickness. Thanks to their atomic thickness and 2D aspect ratio, 2D materials are good candidates for preparing ultrathin membranes with sub-50 nm thickness. However, membranes that are too thin can easily deteriorate due to insufficient rigidity or present pinholes, which results in a short membrane cycling life or lower selectivity performance. In addition, the fabrication of large-area ultrathin membranes is prone to generating defects, thus reducing ion rejection. Thick membranes exhibit poor water permeability because it increases the penetration resistance of water molecules. During membrane engineering, the thickness can be optimized by tuning the total amount of raw materials.

SYNTHESIS OF TMDC MEMBRANE MATERIALS

High-yield and low-cost production of TMDC nanosheets are important for TMDC membrane fabrication. In the past few decades, many preparation methods have been explored, such as top-down (e.g., liquid exfoliation method) and bottom-up strategies (e.g., chemical vapor deposition [CVD], hydrothermal, and solvothermal methods).

As mentioned in the introduction, bulk TMDCs are composed of sandwiched monolayer MX_2 stacked together by van der Waals forces. The relatively weak interaction between MX_2 layers renders them easy to exfoliate by exerting an external force. Thus, a liquid exfoliation method is preferred for the large-scale synthesis of monolayer or few-layered TMDCs. Furthermore, the CVD approach has also been introduced to synthesize TMDC nanomaterials considering the atomic-level fabrication strategy. The quality of TMDCs prepared by CVD is usually high, but their yield is low. Similarly, the composition of TMDCs synthesized by hydrothermal and solvothermal methods is often complicated because both 2H and 1T phases coexist in the product. Apart from the preparation of TMDC nanosheets, we also summarized the preparation methods of TMDC-based membranes in this section, such as filtration, layer-by-layer assembly, Langmuir-Blodgett (LB) deposition, and casting and spin coating methods.

TMDC nanosheet fabrication

Top-down method: Liquid exfoliation

The liquid exfoliation for the preparation of TMDC nanosheets involves two steps (Figure 4A). The first step is intercalation, with the aim of expanding the interlayer spacing of TMDCs by intercalating various species. The reported intercalants include molecules,[57,58] anions,[59–61] and cations.[62–64] The intercalation process is
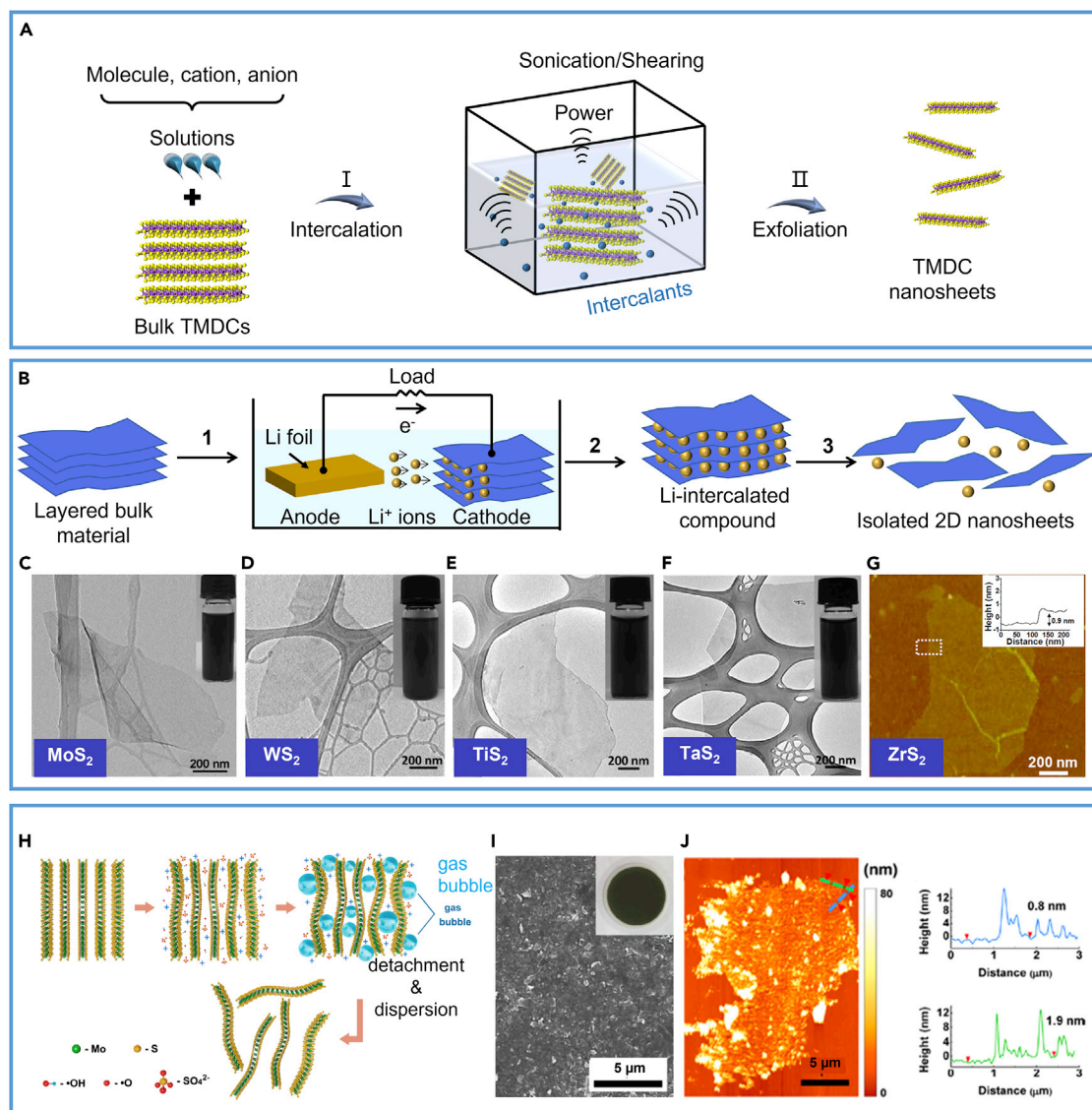
Figure 4. The synthesis of TMDCs nanosheets via top-down methods

(A) Schematic illustration of top-down method for preparing TMDC nanosheets.

(B) Schematic illustration of an electrochemical-assisted intercalation liquid exfoliation method for fabricating TMDC nanosheets.

(C–F) The TEM images and optical images of the obtained single-layer TMDCs (C) (MoS_2), (D) (WS_2), (E) (TiS_2), and (F) (TaS_2) nanosheets are displayed.

(G) AFM image of ZrS_2 is displayed.[65] Copyright 2011, Wiley-VCH.

(H–J) (H) Schematic illustration of mechanism for salt-assisted electrochemical exfoliation of TMDCs, the morphology of exfoliated MoS_2 including (I) SEM image and optical image, (J) AFM topography, and height profiles along the blue and green dashed lines in the AFM image are shown.[66] Copyright 2014, American Chemical Society.

driven by external forces, such as heating or discharge processes. The influencing factors include solvent species, current density, voltage, and discharging time.

The second step is exfoliation, in which the weak van der Waals force between neighboring TMDC layers breaks in solvents with the assistance of external power, such as ultrasound or shearing force. The influencing factors include solvent, surfactant, and sonication conditions. Sonication time has been extensively reported to tune the size and morphology of exfoliated TMDC nanosheets.[67,68] In shearing exfoliation, the lateral shear force generated by shear devices overcomes van der Waals force

between neighboring X-M-X layers.[69] After exfoliation, different lateral sizes of the TMDC nanosheets can be separated by centrifugation.

Alkali metal ions are normally used to assist intercalation in liquid exfoliation. n-Butyllithium (n-BuLi) was first used as an intercalant for exfoliation, in which bulk TMDCs were immersed in n-BuLi/hexane solution before sonication in water.[70] For this method, a large amount of hexane solvent was used to remove excess n-BuLi and other organic residues. In 2011, Zeng et al. prepared a series of single-layer TMDCs (e.g., MoS_2, WS_2, TiS_2, ZrS_2, and TaS_2) via a lithium electrochemical intercalation and exfoliation method (Figure 4B).[65] This method can monitor and finely control the Li^+ intercalation amount by controlling the discharge process. The obtained MoS_2 nanosheets typically have a lateral size of several hundred nanometers with a hexagonal lattice structure (Figure 4C). Remarkably, the yield of single-layer MoS_2 was 92%. This method has also been applied to prepare other single-layer TMDC nanosheets, such as WS_2, TiS_2, TaS_2, and ZrS_2 (Figures 4D–4G). The 2D nature of the single-layer WS_2, TiS_2, ZrS_2, and TaS_2 nanosheets were also confirmed. In addition, Zeng and co-workers further investigated the intercalation mechanism of this method using an *in situ* liquid-cell TEM technique and captured the composition and morphology evolution during the lithiation/delithiation process of MoS_2 nanosheets.[71,72]

Salts could be used to assist intercalation in electrochemical exfoliation method. For example, Lee and co-workers synthesized high-quality MoS_2 nanosheets with the largest lateral size up to 50 μm in Na_2SO_4 solution (Figure 4H).[66] The released O_2 and/or SO_2 gas bubbles expand the interlayer distance to exfoliate the MoS_2 nanosheets. Photographs of the MoS_2-based membrane obtained by vacuum filtration revealed a smooth plane. Scanning electron microscopy (SEM) and atomic force microscopy (AFM) images reveal a rough surface of the membrane assembled by MoS_2 monolayer (~0.8 nm) and bilayer (~1.9 nm) nanosheets (Figures 4I and 4J). The inset of Figure 4I shows a photograph of the MoS_2-based membrane obtained by vacuum filtration. Compared with the electrochemical lithium intercalation and exfoliation method developed by Zeng et al., this electrochemical exfoliation method can also operate in an aqueous solution in an open environment. However, the yield of MoS_2 nanosheets was too low (~5%–9%), and some non-exfoliated MoS_2 thick layers still existed in the final product.

Recently, detailed intercalation and exfoliation processes to construct layered TMDC nanomaterials have been comprehensively reviewed by our group.[73] We summarized the intercalant species and controllable conditions during the intercalation process, the driving force, and influencing factors for the exfoliation process. The morphology, structure, and applications of the obtained 2D TMDC nanomaterials were also reviewed. The intercalation mechanism was also introduced based on kinetic and thermodynamic considerations.

Bottom-up method: Hydrothermal, solvothermal, and CVD methods

Typically, hydrothermal and solvothermal methods are mainly bottom-up methods for obtaining TMDC nanosheets. MoS_2 and WS_2 nanostructures were obtained by reacting molybdate and tungstate precursors, such as $Na_2MoO_4 \cdot 2H_2O$,[74,75] $(NH_4)_8Mo_7O_{24} \cdot 4H_2O$,[76,77] and $(NH_4)_{10}W_{12}O_{41} \cdot H_2O$,[78] with a sulfur source, such as thiourea and thioacetamide, in water or organic solvents. The TMDC nanomaterials obtained through this solution-phase reaction typically exhibit a thin nanosheet or thick layer morphology. Many researchers have investigated the influence of reactant activity and synthetic conditions on TMDC morphology and structure. For
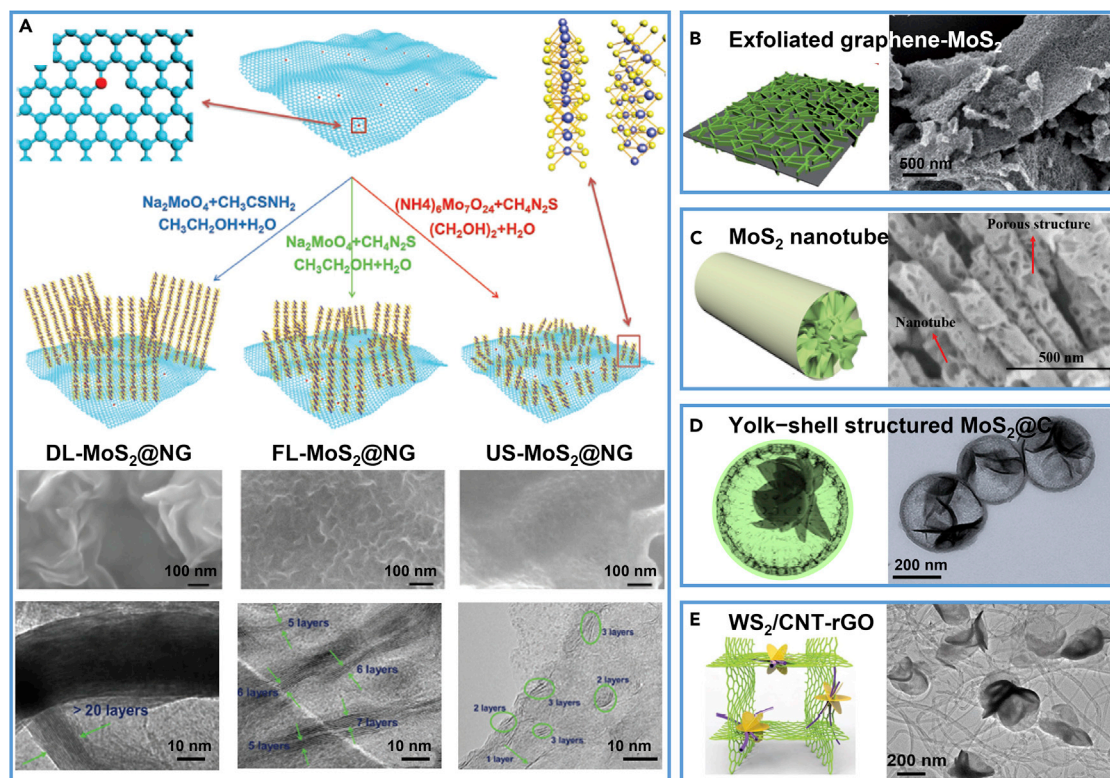
Figure 5. The synthesis of TMDCs nanosheets via bottom-up methods

(A) Schematic illustration of hydrothermal methods for fabricating MoS_2 nanosheets with various morphologies.[79] Copyright 2018, Wiley-VCH.

(B) Schematic illustration and SEM image of exfoliated graphene-supported MoS_2 nanosheets.[80] Copyright 2018, Wiley-VCH.

(C) Schematic illustration and SEM image of porous MoS_2 nanotubes.[81] Copyright 2018, Wiley-VCH.

(D) Schematic illustration and TEM image of yolk-shell structured MoS_2@C spheres.[82] Copyright 2017, American Chemical Society.

(E) Schematic illustration and TEM image of WS_2/CNT-rGO composites.[83] Copyright 2016, Wiley-VCH.

example, Yu and co-workers utilized molybdenum and sulfur sources in solvents to synthesize MoS_2 nanosheets via the solvothermal method (Figure 5A).[79] Dozen-layered, few-layered, and ultra-small MoS_2 nanosheets were successfully deposited on N-doped graphene substrates. Similarly, hydrophilic MoS_2 nanosheets were vertically grown on the surface of hydrophobic exfoliated graphene during the solvothermal process (Figure 5B).[80] Various morphologies of TMDC nanomaterials can be fabricated by adding particular templates to the hydrothermal and solvothermal reaction systems (Figures 5C–5E).[81–83] Moreover, the relationship between the structure and product performance, rather than morphology control, is important to scientific research.

The chemical, mechanical, and structural stability of materials impact the cycling life of water purification membranes. Guo et al. synthesized MoS_2 thick layers by a hydrothermal method (hydro-MoS_2) and treated them with a "supportive" drying process, which achieved a mean interlayer spacing of ~1 nm.[84]

In general, the morphology and component controllability are the significant advantages of hydrothermal, solvothermal-based solution methods. However, the long preparation time, and high-temperature and high-pressure requirements, hinder their applications. Meanwhile, hydro- and solvo-thermal reactions are performed in a closed system, which limits researchers in the observation of their growing process.
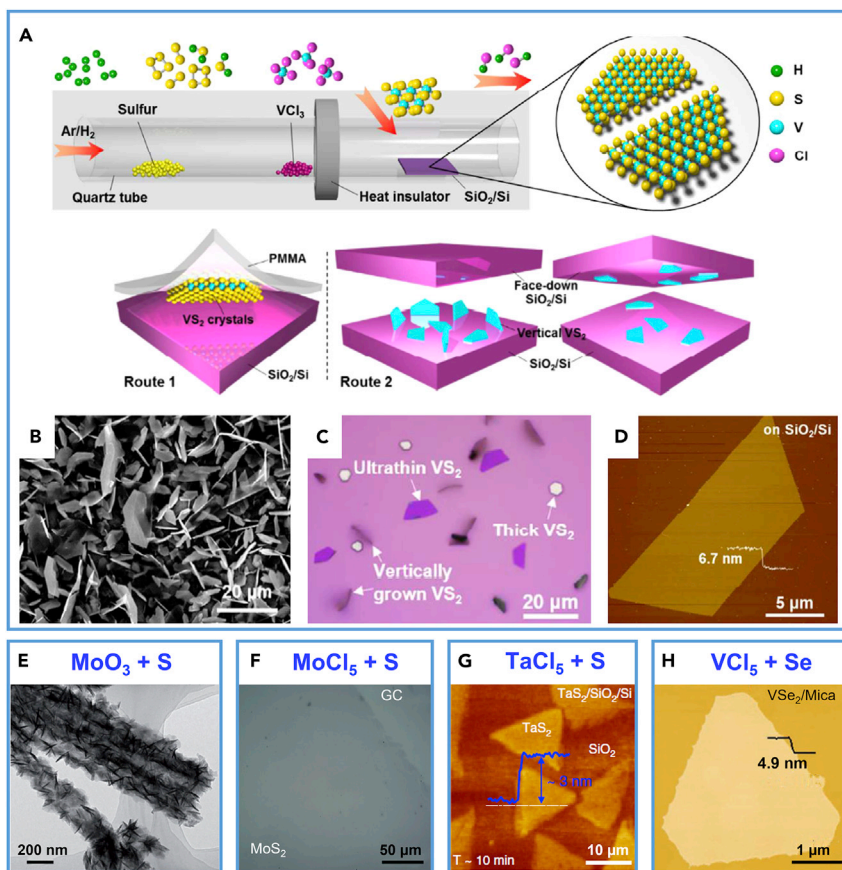
Figure 6. The synthesis of TMDCs nanosheets via the CVD method

(A) Schematic illustration of CVD method for fabricating VS$_2$ nanosheets.

(B–D) (B) SEM, (C) optical, and (D) AFM images of VS$_2$ nanosheets.[85] Copyright 2017, American Chemical Society.

(E) TEM image of MoS$_2$ tubes synthesized using MoO$_3$ as the molybdenum source.[86] Copyright 2018, Wiley-VCH.

(F) SEM image of MoS$_2$ nanosheets synthesized using MoCl$_3$ as the molybdenum source.[87] Copyright 2020, American Chemical Society.

(G) AFM image of TaS$_2$ nanosheets synthesized using TaCl$_5$ as the tantalum source.[88] Copyright 2017, Springer Nature.

(H) AFM image of VSe$_2$ nanosheets synthesized using VCl$_5$ as the vanadium source.[89] Copyright 2017, Wiley-VCH.

In the CVD method, gas-phase compounds (e.g., sulfur, selenium, and metal precursor) react with substances and form 2D TMDCs nanosheets. The substrate includes SiO$_2$/Si, mica, sapphire, soda-lime glass, and Au foils. The obtained TMDC nanosheets are removed from the substrates using a polymer-assisted transfer method. For example, Zhang and co-workers synthesized metallic vanadium disulfide (VS$_2$) nanosheets using VCl$_3$ as a vanadium source, which reacted with sulfur under H$_2$/Ar gas flow (Figure 6A).[85] Ultrathin VS$_2$, vertically grown VS$_2$, and thick VS$_2$ co-existed on the SiO$_2$/Si substrate (Figures 6B and 6C). They transferred these VS$_2$ nanosheets onto arbitrary substrates using a polymethyl methacrylate-assisted transfer process. The obtained VS$_2$ nanosheets had thicknesses of sub-10 nm and lateral sizes of tens of micrometers (Figure 6D). In addition, MoS$_2$ nanothorns, which were epitaxially grown on the surface of carbon nanotubes using MoO$_3$ as a molybdenum source, prevented the aggregation of MoS$_2$ nanosheets during lithium charge/discharge processes (Figure 6E).[86] Chlorides are the most commonly used

precursors in the CVD process for the preparation of low-porosity and high-purity TMDCs (Figures 6F–6H).[87–89] The crystal phases (2H and 1T phases) and size of nanosheets can be precisely tuned.

Recently, two new substrates (salts and diatomite) were used to fabricate TMDC nano-materials via the CVD method.[90] For example, Zhang and co-workers synthesized high-quality metallic TMDC (e.g., TaS_2 and NbS_2) nanosheets in large scale by using a NaCl template.[91] This synthetic route is compatible with the water dissolution-filtration process, which can be used with high-efficiency adsorbents for organic dyes.[92] Despite these advances, the CVD method has some disadvantages, such as the high cost of instruments and noxious gaseous by-products, which hinder the industrialization of this technique. Efforts should be made to develop more effective approaches.

Generally, for synthesizing TMDC nanosheets, the CVD method is utilized to fabricate TMDC nanosheets with specific sizes and features that satisfy the requirements of catalytic applications, where TMDC sheets are not limited to aspect ratio and thickness. In contrast, hydrothermal and solvothermal methods are used to generate TMDC nanosheets with a relatively low aspect ratio and high thickness. The liquid exfoliation method was used to obtain TMDC nanosheets with a high aspect ratio in the range of 10^2–10^3 and a small thickness of <5 nm. In particular, the electro-chemical intercalation and liquid exfoliation method is an effective strategy for the mass production of single-layered TMDC nanosheets.

Preparation of TMDC-based membranes

After introducing various preparation methods for TMDC nanosheets, we need to specify the preparation of suitable TMDC-based membranes for water purification. Except for atomically thin TMDC membranes prepared by the CVD method, current studies on TMDC-based membranes have mainly focused on 2D laminar membranes constructed by stacking exfoliated high aspect ratio nanosheets. It is critical to stack the nanosheets into a specific orientation and control their interlayer distance, which can act as channels to separate fluid from pollutant ions or particles. The preparation methods for TMDC laminar membranes include filtration, layer-by-layer (LBL) assembly, LB deposition, casting, and spin coating. The detailed procedures of these methods are discussed in the following section.

Filtration

Filtration, particularly vacuum filtration, is a facile and highly scalable method for preparing 2D TMDC laminar membranes. This process involves loading TMDC nanosheets onto porous polymeric/inorganic supports. The pore sizes of these supports are usually >200 nm. The entire filtration system is displayed in Figure 7A. During filtration, a wet membrane was formed on the surface of supports, which was clamped between the filter holder and glass funnel (Figure 7B). The size of the obtained laminar membrane was determined by the effective filtrated area of the support during the filtration process. The thickness of the obtained laminar membrane can be controlled by tuning the concentration and volume of the TMDC nanosheets.

Hirunpinyopas et al. exfoliated MoS_2 thick layers stacked together disorderly on a poly(vinylidene fluoride) (PVDF) substrate, forming a laminar membrane with a thickness of ~5 μm (Figure 7C).[93] In another study, completely dried MoS_2 and fully hydrated MoS_2 membranes were constructed via a pressure-assisted filtration method on a poly(ethersulfone) (PES) support (Figure 7D).[94] Also, researchers stacked WS_2 nanosheets on an anodic aluminum oxide (AAO) support to obtain a lamellar membrane via the vacuum filtration process (Figure 7E).[95] The thicknesses
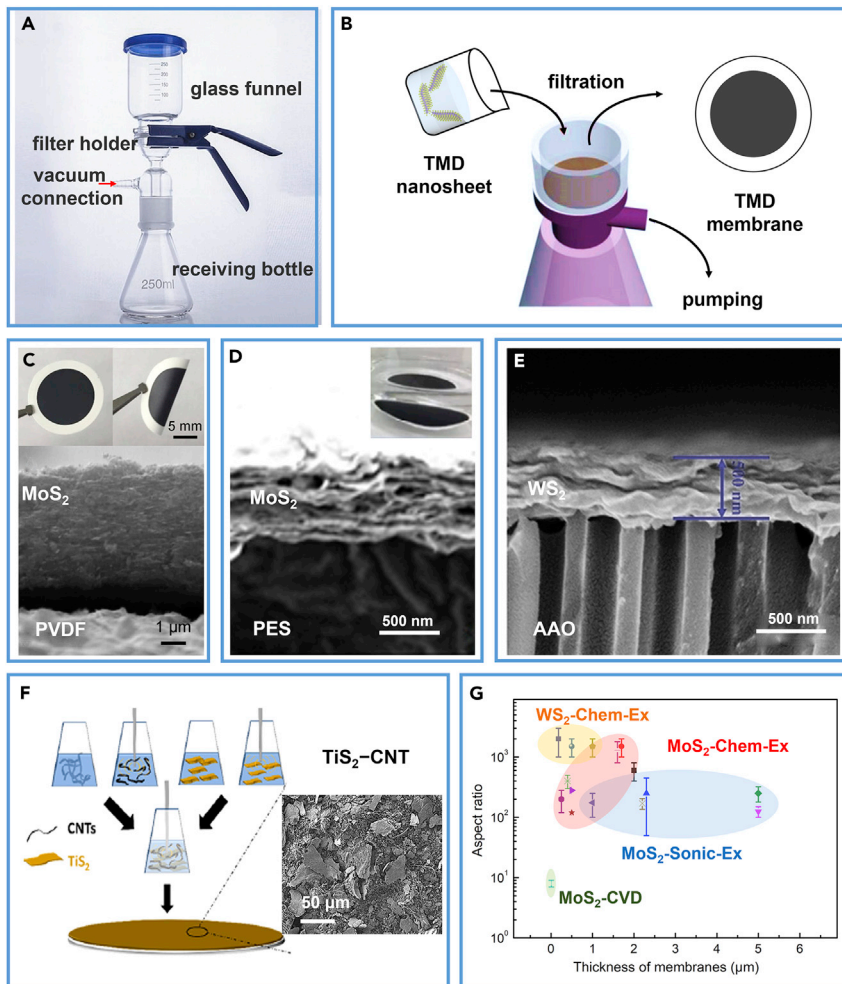
Figure 7. The fabrication of TMDC-based membranes via the filtration method

(A) Image of the filter system for fabricating membranes.

(B) Schematic illustration of filtration procedures of TMDC-based membranes: (1) pour TMDCs nanosheet dispersion into funnel; (2) pump to filtrate the membrane; and (3) transfer TMDC membrane.

(C) Photograph and cross-sectional SEM image of MoS_2 membranes supported by PVDF.[93] Copyright 2017, American Chemical Society.

(D) Photograph of MoS_2 membranes in water and SEM image of MoS_2 membrane supported by PES.[94] Copyright 2017, American Chemical Society.

(E) SEM image of WS_2 membranes supported by AAO.[95] Copyright 2018, Wiley-VCH.

(F) Schematic illustration and SEM image of MoS_2/CNT.[96] Copyright 2017, American Chemical Society.

(G) Comparison of the aspect ratio and the thickness of TMDC-based membranes applied in water desalination.

of the WS_2 membrane and WS_2 nanosheets were ~500 and 1.2 nm, respectively. Presser and co-workers applied blending and filtration method for preparing TiS_2/CNT membrane for brackish and seawater desalination for the first time (Figure 7F).[96] The mixing of carbon-based materials with TMDCs can substantially improve the mechanical property and flexibility of the membranes and thus increase their stability.

Typically, ultrathin nanosheets (single layer or few layers) with a high aspect ratio can easily construct thinner membranes, while thick layers form thicker films. Most

studies on TMDC-based laminar membranes applied in water desalination and purification are assembled using high aspect ratio (e.g., 100–2,000) TMDC nanosheets obtained by the liquid exfoliation method (Figure 7G). The membrane thickness varies from hundreds of nanometers to several micrometers. Compared with dense and thick membranes, water molecules can easily penetrate through thinner membranes with low density. Thus, ultrathin and stable lamellar membranes can help achieve efficient water purification.

LBL assembly and LB deposition

LBL assembly is an approach to develop an ultrathin film on solid support by alternate exposure to positive and negative species with spontaneous deposition of the oppositely charged ions.[97] The thickness of LBL membranes can be controlled by the amount of the coating materials. The driving force of the LBL assembly is ascribed to electrostatic interactions, hydrogen bonding, and other molecular interactions (e.g., charge-transfer interactions, covalent bonding, and coordination interactions).[98] Recently, an increasing number of studies have focused on using LBL assembly method to fabricate TMDC-based membranes for various applications. For example, Li et al. incorporated MoS_2 nanosheets into poly(ethyleneimine)/poly(acrylic acid) (PEI/PAA) active layer, which is loaded on the surface of PES support layer through LBL assembly method (Figure 8A).[99] The obtained PEI/PAA/MoS_2 active layer exhibited a lamellar structure with thickness of around 45 μm. The membrane thickness is around 180 μm. Recently, Kang et al. prepared wafer-scale WS_2/MoS_2/$MoSe_2$ heterostructures, which are freed from the restriction of lattice match or alignment, via the LBL assembly method at the atomic scale (Figure 8B).[100] The authors used a programmed vacuum stacking process to solve air-trapped bubble-like structure problems and generate well-aligned WS_2/MoS_2/$MoSe_2$ flat films. Another study reported a poly(sulfobetaine methacrylate)/polydopamine/MoS_2 (PSBMA/PDA/MoS_2) nanofiltration membrane for the separation of dye/salt.[101]

The LB deposition technique is a way of creating a supra-molecular assembly in ultrathin films with a controlled layered structure and crystal parameter,[104] which is another controllable method to prepare TMDC-based membranes. LB deposition is performed in three steps, solution spread, compression, and film transfer, as shown in Figure 8C. There are two precipitation modes when transferring the LB film from water surface to substrate surface, i.e., vertical precipitation and horizontal precipitation. Pope and co-workers adopted an LB deposition technique to prepare uniform and large-area MoS_2 films by using a dimethylformamide/1,2-dichloroethane mixture as the spreading solvent.[102] This solvent enables the suspended nanosheets to float on the water surface without losing material into the aqueous sub-phase. After observing that MoS_2 nanosheets aggregated into islands, and then grew into a locally uniform film covering ~50% of the LB trough surface, they used moveable barriers to compress floating MoS_2 nanosheets into a densely tiled film and simultaneously collected the surface pressure-area (π-A) isotherm (Figure 8D). The optical images show that the MoS_2 film remained stable at the air-water interface and a clear film boundary is formed. The MoS_2 film was transferred on a glass substrate by a horizontal precipitation method and the film area reached 130 cm^2. SEM and AFM images show that the MoS_2 film is composed of high-density tiled sheets.[103] This LB deposition technique allows facile fabrication of highly ordered thin films at the molecular level.

Overall, both LBL assembly and LB deposition techniques are facile methods to fabricate TMDC-based membranes with controlled thickness and size. These methods are facile for large-scale production using simple instrument, which are
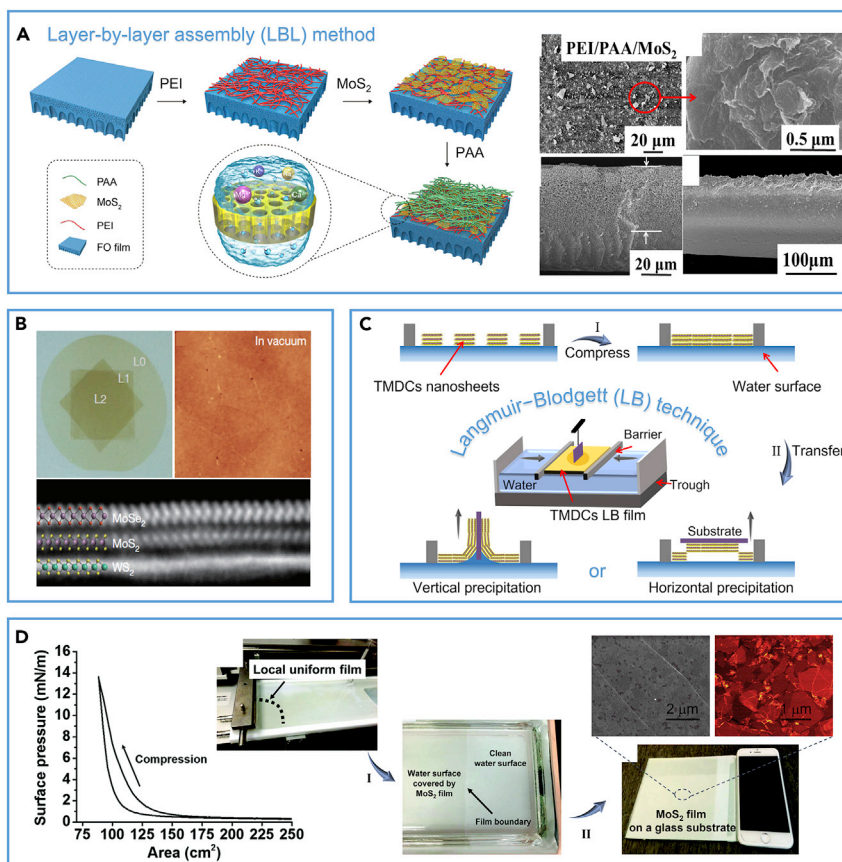
Figure 8. The fabrication of TMDC-based membranes via LBL assembly and LB deposition methods

(A) Schematic illustration of LBL assembly method for preparing the PEI/PAA/MoS$_2$ film, and its surface and cross-section SEM images.[99] Copyright 2018, Elsevier.

(B) Optical image (left), AFM image (right) of wafer-scale MoS$_2$ films, and cross-sectional STEM image of three-layer MoSe$_2$/MoS$_2$/WS$_2$ film.[100] Copyright 2017, Springer Nature.

(C) Schematic illustration of Langmuir-Blodgett deposition technique for preparing TMDCs film.

(D) Surface pressure versus area isotherm of MoS$_2$ nanosheets during compression process.[102] Copyright 2017, Royal Chemical Society. Photograph of MoS$_2$ nanosheets floating on the water surface (before compression), a stable MoS$_2$ thin film floating on the water surface (after compression), and a large-area MoS$_2$ film on a glass substrate deposited by the horizontal precipitation method (after transfer). A smartphone is used for comparison purpose. SEM and AFM images (right side at the up position) show the surface morphology of the obtained film.[103] Copyright 2020, American Chemical Society.

beneficial for practical application. Nevertheless, there are some disadvantages for these two methods, such as patchwise depositions and occasional generation of folded sheets, which lead to uneven films. Despite the disadvantages, LBL assembly and LB deposition methods are still powerful techniques in developing high-performance TMDC-based membranes for water purification in the future.

Casting and spin coating

Casting is a simple technique to fabricate thin films. However, the obtained films are not uniform. To solve this problem, Van der Bruggen and co-workers fabricated a hydrophilic MoS$_2$-PSBMA/PES membrane via alternatively casting PES and exfoliated MoS$_2$-modified PSBMA on a transparent glass (Figure 9A).[105] Also, they filtered the casting solution as well as using a scraper to obtain uniform casting liquid and film.
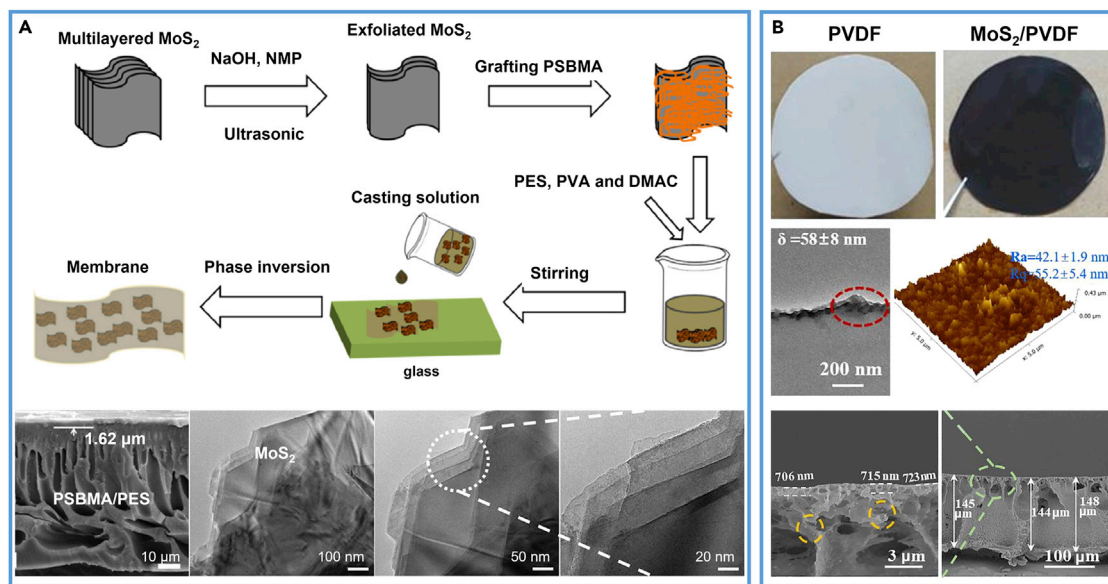
Figure 9. The fabrication of TMDC-based membranes via the casting method

(A) Schematic illustration of casting method for fabricating MoS₂ membranes; SEM and TEM images of PSBMA/PES supported MoS₂ membrane.[105] Copyright 2019, Elsevier.

(B) Photographs, TEM, AFM, and SEM images of the as-prepared MoS₂/PVDF membrane.[106] Copyright 2021, Elsevier.

Xia and co-workers fabricated a MoS₂/PVDF membrane with a thickness ranging from 500 to 720 nm using a casting method (Figure 9B).[106] The average roughness of the MoS₂/PVDF membrane fabricated with 0.75 wt % MoS₂ in the casting solution is 42.1 ± 1.9 nm.

Spin coating is a procedure used to deposit uniform thin films onto flat substrates. Usually a small amount of coating material is first applied on the center of the substrate, which is either spinning at low speed or not spinning at all. The substrate is then rotated at a speed of up to 10,000 rpm to spread the coating material by centrifugal force. Hence, spin coating is similar to the casting method but with additional external force (e.g., centrifugal force), and the uniformity of the film prepared by spin coating method is better than the casting method. The viscosity and surface tension of the coating materials are two main factors that affect the thickness and uniformity of the films. Here, MoS₂ ultrathin films on a 2-inch SiO₂/Si substrate have been successfully prepared by this method.[107]

TMDC-BASED MEMBRANES FOR WATER DESALINATION

TMDC-based membranes exhibit great promise for water desalination owing to their unique chemical and physical properties, such as superior elasticity and flexibility, 2D channels, and extraordinary stability in aqueous environments. Moreover, the ultrathin thickness and tunable space between MX₂ layers provide notable advantages for ion/molecule sieving. To date, both experimental and theoretical research on laminated membranes based on MoS₂, WS₂, and TiS₂ nanosheets have been reported for water purification, as shown in Figure 10. In the past decade, most of these studies (nearly 80%) focused on MoS₂-based membranes used for RO, FO, and nanofiltration technologies. Few studies have involved STD and CDI technologies. In addition, some researchers have focused on modifying TMDC-based membranes for improved water desalination performance.
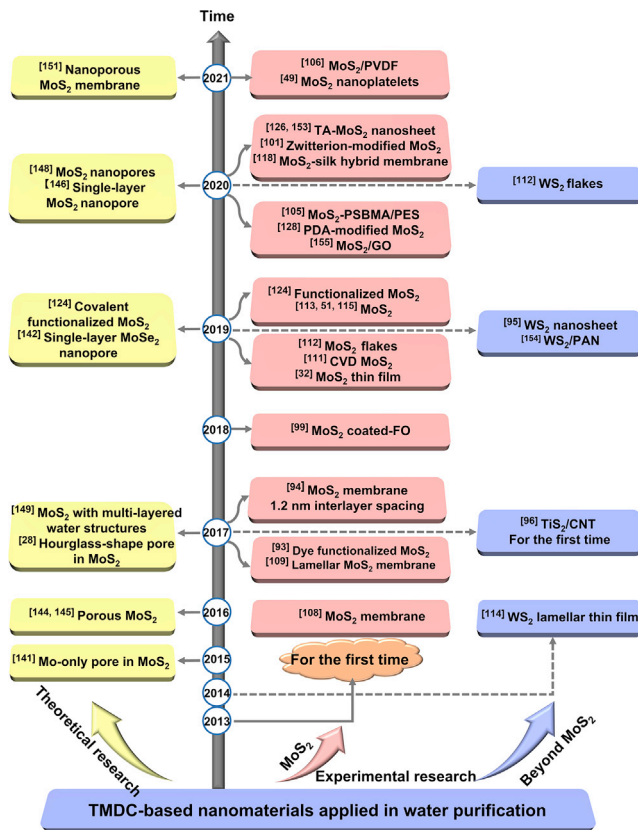
Figure 10. Timeline of the representatively reported 2D TMDC-based membranes applied in water desalination

MoS₂

Among all 2D TMDC nanomaterials applied in water purification technology, MoS_2 has been intensively investigated as a promising candidate. In 2013, Peng and co-workers used MoS_2 nanosheets to fabricate a laminar membrane for water purification for the first time.[108] They found that the obtained MoS_2 membrane, with a thickness of $1.7 \pm 0.6 \, \mu m$, exhibited a water flux of $245 \, L \, h^{-1} \, m^{-2} \, bar^{-1}$, which is three to five times higher than that of GO membranes (Figure 11A). Subsequently, Park and co-workers constructed a MoS_2 lamellar membrane using angstrom-sized 2D layered MoS_2 platelets (Figure 11B).[109] This lamellar membrane exhibited a superior lifespan in an aqueous environment with wide pH values, and simultaneously demonstrated good sieving properties toward organic species, gases, and inorganic salts. In 2017, Mi and co-workers reported that the hydrated state of the layer-stacked MoS_2 membrane maintained an expanded interlayer spacing of 1.2 nm, enabling fast water transport and organic dye separation through nanochannels (Figure 11C).[94] Compared with dried MoS_2 and other GO-based membranes, the hydrated MoS_2 membrane produced high ion/molecule rejection and remarkable water permeance ($\sim 250 \, L \, h^{-1} \, m^{-2} \, bar^{-1}$). They proposed that such high performance was attributed to the low hydraulic resistance of MoS_2 nanochannels, together with the synergic effect of size-exclusion and electrostatic repulsion mechanisms. They also applied this layer-stacked MoS_2 membrane to point-of-use devices, exhibiting highly selective removal of Pb^{2+} from drinking water.[110]

In 2019, Jung and co-workers synthesized a centimeter-scale MoS_2 membrane by the CVD method (Figure 11D), greatly promoting the commercialization process
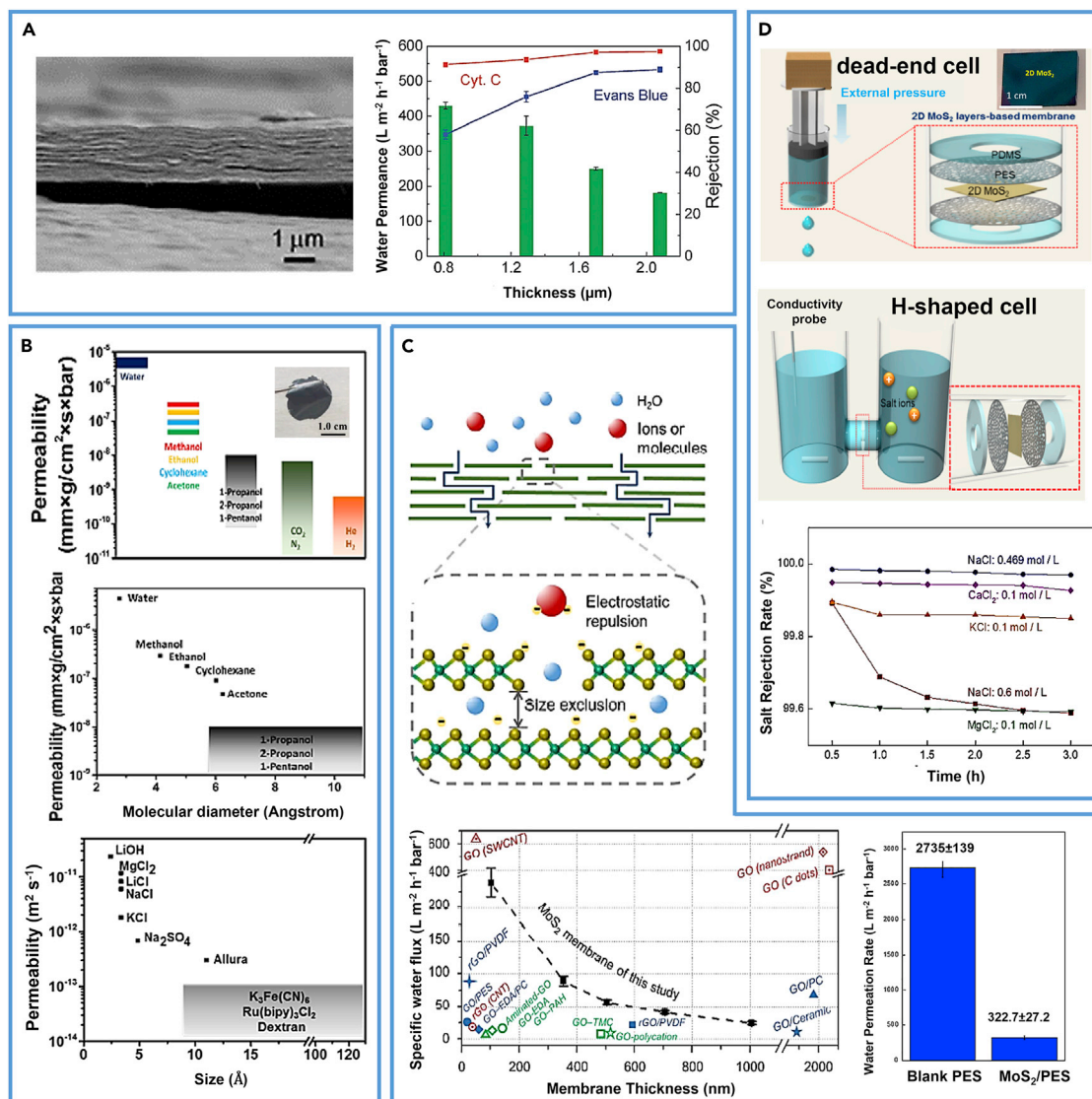
Figure 11. The desalination performance of MoS$_2$ membranes

(A) Cross-sectional SEM image of the MoS$_2$ membrane and its water flux and dye rejection performance.[108] Copyright 2013, Royal Chemical Society.

(B) Permeability of liquids and salts through the stacked MoS$_2$ membrane.[109] Copyright 2017, American Chemical Society.

(C) Proposed sieving mechanisms of the MoS$_2$ membrane and its water desalination performance.[94] Copyright 2017, American Chemical Society.

(D) Schematic setup for water permeation and salt rejection measurements, and the water permeation rate results.[111] Copyright 2019, American Chemical Society.

of TMDC-based membranes.[111] The thickness of the obtained MoS$_2$ membrane was only ~7 nm. To measure the desalination performance, layered PDMS/PES/MoS$_2$/PES/PDMS membranes were assembled in a dead-end filtration cell and an H-shaped cell, respectively. They found that the obtained MoS$_2$ membrane exhibited extraordinary water flux (>322 L h^{-1} m^{-2} bar^{-1}) and high ion rejection for various mineral salts (>99%) owing to the ultrathin thickness and high-density ''intrinsic'' structural imperfections.

Meanwhile, some researchers discovered that the stacking configuration of nanosheets affects membrane permeability and selectivity. For example, Wang and co-workers stacked irregular MoS$_2$ nanosheets to form a porous membrane with

hierarchical channels configured by narrow gaps (~1.8 nm) and large cavities (~8.3 nm).[112] They found that these hierarchical channels clearly enhanced the water permeance (>1430 L h^{-1} m^{-2} bar^{-1}) and reduced the dye rejection (~90%). In other words, imperfect stacking laminates sacrificed ion/molecule rejection to increase the total water flux. Elimelech and co-workers demonstrated that the nanosheets stacking behavior of MoS$_2$ membrane could affect its selectivity and separation performance based on experiments results.[113] The theoretical simulation also showed that, compared with the ideal stacking of nanosheets, a small amount of imperfect stacking in MoS$_2$ laminate membranes, which was believed to form hierarchical channels and thus benefit water flux increases, actually reduced the membrane's selectivity due to the formation of porous structure. Meanwhile, both the PVDF substrate and MoS$_2$ membrane exhibited similar poly(ethylene oxide) (PEO) molecule rejection. This research provides insight into understanding and clarifying the role of lamellar MoS$_2$ in 2D desalination membranes. Given this, it would seem reasonable to suggest the development of a well-controlled fabrication process to carefully tune the lamellar structure to acquire highly selective 2D desalination membranes.

Beyond MoS$_2$ (i.e., WS$_2$ and TiS$_2$)

In 2014, following a previously reported methodology for the synthesis of MoS$_2$ membranes, Peng and co-workers further reported a WS$_2$ laminar film with a thickness of 500 nm for water desalination (Figure 12A).[114] Benefiting from the nanostrand channels, the obtained WS$_2$ membrane exhibited 2-fold enhancement in water flux and the same level of ion rejection compared with the MoS$_2$ membrane. This work broadens the selection range of 2D TMDC-based nanomaterials for seawater desalination membranes. In 2019, Lang and co-workers synthesized WS$_2$-based laminar membranes exhibiting good stability (the membranes changed slightly after soaking in water for 28 days) and antibacterial properties.[95] In 2020, Liu and co-workers filtrated WS$_2$ nanosheets with lateral sizes (<100 nm) on a nylon support to increase the mechanical properties of membranes (Figure 12B).[115] The membrane exhibited a water flux of >800 L h^{-1} m^{-2} bar^{-1} and could reject ~99% of dye molecules, such as rhodamine-B and Evans blue. This high performance was attributed to the WS$_2$ nanosheet forming nanochannels and nanocapillaries, which reduced the average length of the water transport paths. This work provides an avenue for selecting promising TMDC-based candidates for application in dye desalination.

Similarly, hybrid membranes composed of WS$_2$ nanosheets incorporated into polyelectrolytes have been designed to enhance the dye/salt separation efficacy. Lang and co-workers investigated the dye desalination performance of WS$_2$ membranes constructed on PA and AAO substrates (Figures 12C and 12D).[116] They discovered that, compared with WS$_2$/AAO, the WS$_2$/PA membrane provided a larger interlayer spacing of 1.18 nm and more defects/pores, causing a high Rose Bengal rejection of 98.5% and high water permeance of 597 L m^{-2} h^{-1} bar^{-1}. Recently, a PAA/WS$_2$/poly(diallyldimethylammonium chloride) hybrid membrane was fabricated to enhance the dyes (e.g., Congo red and reactive black 5)/NaCl separation efficacy (Figure 12E).[117] Benefiting from the increased hydrophilicity and surface negativity, the obtained hybrid membrane reached high dye/salt separation efficiency. Unfortunately, the water flux of these membranes decreased with increasing filtration test time, showing a trade-off between dye/salt selectivity and water permeance.

In addition to MoS$_2$ and WS$_2$, Presser and co-workers explored TiS$_2$ for Na$^+$ removal in aqueous electrolytes for seawater desalination.[96] An asymmetric cell, assembled using a TiS$_2$-CNT hybrid electrode and a microporous activated carbon cloth, exhibited high charge efficiency over 70 cycles at 600 mM NaCl solution. This novel
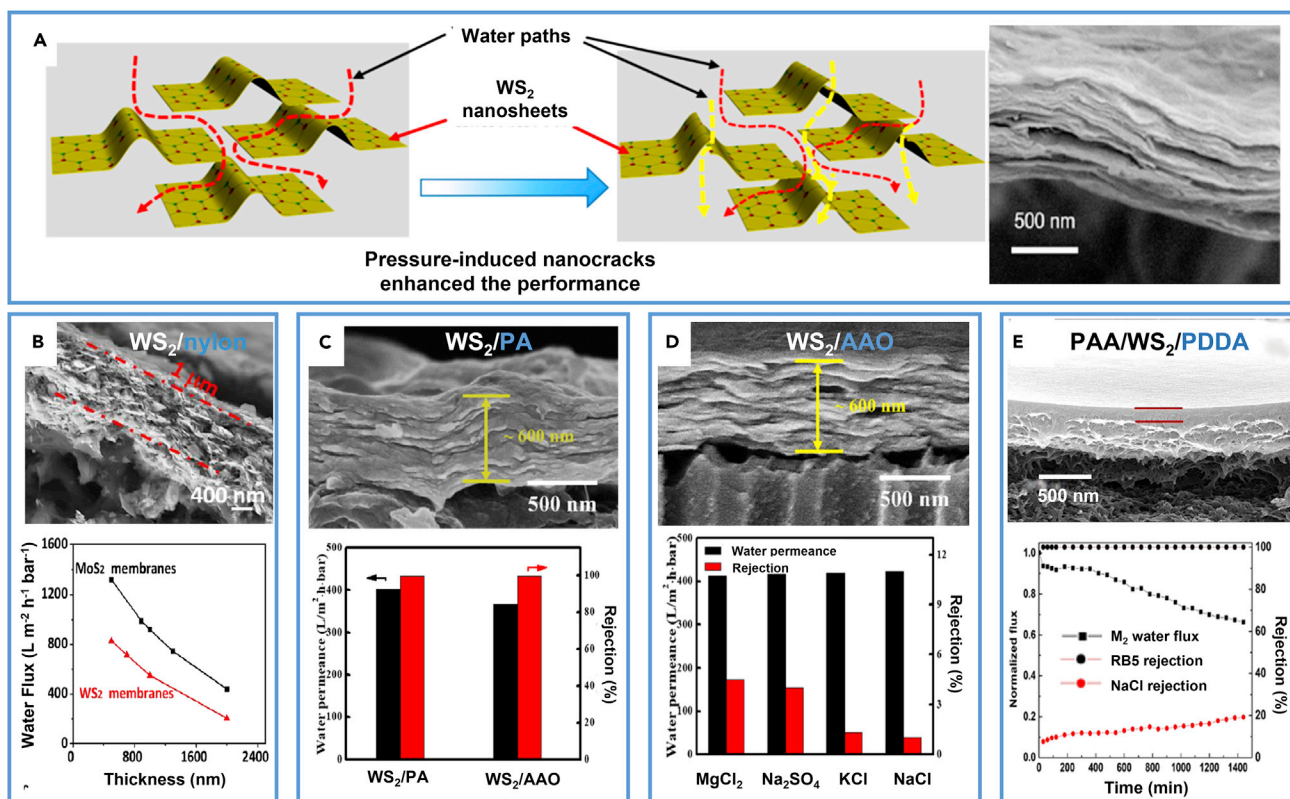
Figure 12. The desalination performance of membranes beyond MoS$_2$

(A) Schematic illustration of water paths in WS$_2$ membranes and their cross-sectional SEM image.[114] Copyright 2014, American Chemical Society.
(B) Cross-sectional SEM image of WS$_2$/nylon membrane and their water flux at different thicknesses.[115] Copyright 2020, American Chemical Society.
(C and D) Cross-sectional SEM image of (C) WS$_2$/PA and (D) WS$_2$/AAO membranes and their water desalination performance.[116] Copyright 2020, Elsevier.
(E) Cross-sectional SEM image of WS$_2$/poly(diallyldimethylammonium chloride) (PDDA) and its desalination performance.[117] Copyright 2020, American Chemical Society.

approach of membrane-free hybrid faradic CDI paves the way for energy-efficient desalination of seawater.

Overall, in the field of water desalination and treatment, TMDC-based membranes exhibit relatively high water permeance and potential sieving performance for mineral salts, organic dyes, and other micropollutants. As shown in Tables 1 and 2, these TMDC-based membranes achieved high water flux of up to several hundred liters per square meter per hour per bar (equivalent to ∼100 gal/day). Their salt and dye rejection was >70%, and some even reached 90%. Nevertheless, the selectivity of TMDC-based membranes is unsatisfactory when compared with that of commercial thin film nanocomposites. In addition, we cannot ignore the fact that the working stability of these membranes is only tens of cycles or hours, which is considerably shorter than that of commercial thin film nanocomposites. As mentioned in Performance evaluation criteria, stability is one of the most important performances for semipermeable membranes when considering reducing the cost of commercialization. Therefore, new strategies and approaches are necessary to improve the stability of TMDC-based membranes for water desalination. Furthermore, very few reports are available on the chlorine resistance and boron removal of TMDC-based membranes for water purification. However, halogen elemental chlorine, as well as bacteria, are two factors that cause a semipermeable membrane fouling problem

Table 1. Water desalination and purification performance and salt rejection of reported TMDC-based membranes

Materials	Thickness (μm)	Water flux (L m^{-2} h^{-1} bar^{-1})	Salt rejection (%)	Stability	References
MoS$_2$/PA	0.179	6.2	NaCl: 98.6	retain 99.6% salt rejection for 14 h	Li et al.[32]
Ethyl-2-ol-functionalized MoS$_2$	0.25	∼45	NaCl: 70	no visible macroscopic degradations are observed after several months	Ries et al.[118]
TA-modified MoS$_2$	5	32	K$^+$,Na$^+$,Li$^+$,Ca^{2+}, Mg^{2+}: >97	>80% of the original TA-MoS$_2$ remain dispersed after 150 days	Hu et al.[119]
CV functionalized MoS$_2$	3	40 × 10^{-3}	NaCl: 96.36(±0.27)	no change in liquid water for over 6 months	Hirunpinyopas et al.[93]
SY functionalized MoS$_2$	–	–	NaCl: 97.73 (±0.63)		
MoS$_2$ nanosheets and nanodisks	–	603 ± 38	NaCl: 99	rejection >98% after 5 days of continuous operation	Sapkota et al.[51]
CVD-grown few-layer MoS$_2$	0.007	>322	various cations: 99	–	Li et al.[111]
PSBMA/PDA/MoS$_2$	4.54	262	Na$_2$SO$_4$: 12.9	–	Zhang et al.[101]
MoS$_2$ platelet	–	∼2.2 × 10^{-3}	–	no weight loss after 12 h	Deng et al.[109]
WS$_2$ nanosheets	–	2 orders of magnitude higher than that of commercialmembranes	–	water permeance slightly drops by about 3.1% at pH 2 after 12 h	Sun et al.[114]
TA-modified MoS$_2$	0.07–0.09	7.6	Na$_2$SO$_4$: 96.5 NaCl: 33.8	–	Zhang et al.[120]
TA-modified MoS$_2$	∼0.03	17	Na$_2$SO$_4$: 98.5	salt rejection retained 98% for 120 h	Ma et al.[121]
MoS$_2$/PEI	–	4.6	MgCl$_2$: 95.5	MgCl$_2$ rejection retained for 100 h	Zhang et al.[122]
MoS$_2$/GO	0.3	48.27	Na$_2$SO$_4$: 66.76 NaCl: 56.02 MgCl$_2$: 44.85	retained salt rejection for 5 cycles	Ma et al.[123]

CV, crystal violet; SY, sunset yellow; TA, tannic acid; PTCA, polythiocyanuric acid; PEI, polyethyleneimine; PAN, polyacrylonitrile.

during the generation of drinkable water. Thus, efforts to develop anti-chlorine and antibacterial TMDC-based membranes will be important for extending the lifetime of next-generation semipermeable membranes.

Since the size of channels or pores on TMDC-based membranes has not been tuned, the selectivity of these membranes for salts and small molecular dyes is not ideal. On the other hand, intrinsic channels composed of three-atom-thick layers in TMDC nanosheets are sufficiently small to reject hydrated ions or high weight organic molecules, but they also limit the penetration of water molecules. In addition, some theoretical studies have demonstrated that the single-layer structure of TMDCs readily form pores for rapid water permeation.[27,28] In fact, the experimental construction and structural detection of pores in TMDC nanosheets is fairly challenging. This suggests that further studies are necessary to investigate the relationship between the structure and performance of TMDC-based membranes for water desalination and purification.

Performance improvement strategy

The sieving mechanism of semipermeable membranes is based on the size of channels or pores (i.e., size exclusion) and electrostatic interactions to separate various substances (e.g., hydrated salt ions, heavy metal ions, organic matter, and algal toxins) from undrinkable water.[126,127] Also, the size regimes of micropores and macropores are <2 and >50 nm, respectively. Mesopores are in the range 2–50 nm (Figure 13). TMDCs possess an ideal interlayer spacing in the range 0.6–1.2 nm, which is in the micropore scope. Within this scope, the existing defects on TMDC nanosheets reportedly exhibit excellent catalytic performance.[128,129] However, the nanochannels or pores have not been effectively exploited in the field of water

Table 2. Water desalination and purification performance and micropollutants rejection of reported TMDC-based membranes

Materials	Thickness (μm)	Water flux (L m^{-2} h^{-1} bar^{-1})	Micropollutant rejection (%)	Stability	References
Methyl-functionalized MoS$_2$	2	24($\pm$0.6)	CF: ~93 AP: ~94 β-OD: ~100	no visible macroscopic degradations are observed after several months	Ries et al.[118]
TA-modified MoS$_2$	–	15,000 $\pm$ 100	99.87 $\pm$ 0.1%	–	Hu et al.[119]
MoS$_2$ nanosheets	–	30–250	RD: 90 MB: 40	–	Wang et al.[94]
MoS$_2$ thick layers	–	>1430	>90% (dye size: >1.9 nm)	>97% of the solvent permeance after >24 h in acid/alkaline solution	Cui et al.[112]
WS$_2$ nanosheets	0.5	410	EB: ~95	slight change in the water permeance and the EB rejection after 45 h	Cheng et al.[95]
MoS$_2$ nanosheets	–	918	RB: ~80 EB: ~75	high rejection rate for EB after 10 cycles	Su et al.[115]
WS$_2$ nanosheets	–	828	RB: ~ 96 EB: ~99	–	Su et al.[115]
PSBMA/PDA/MoS$_2$	4.54	262	MB: 99.8	–	Zhang et al.[101]
MoS$_2$ laminar	1.7	245	EB: 89	92.3% of the rejection ratio for EB at pH 2	Sun et al.[108]
WS$_2$/PAN	0.15	43.35	RBBR: 86	~99% Evans Blue rejection after 7 days	Tham et al.[124]
MoS$_2$/GO	0.3	48.27	DR80: 99.99 CR: 99.90 Rh B: 99.76 MB: 99.66	MB rejection retained for 5 cycles	Ma et al.[123]
PTCA-modified MoS$_2$	–	<220	CR: 80	retain 80% heavy metal ions rejection for 12 cycles	Sreeramareddygari et al.[125]

EB, Evans blue; RD, rhodamine; RB, rhodamine-B; MB, methylene blue; TA, tannic acid; CF, caffeine; AP, acetaminophen; β-OD, β-estradiol; RBBR, Remazol Brilliant blue R; CR, Congo red; Rh B, rhodamine-B; DR80, direct red 80.

desalination, although there is a clear possibility of enhancing the selectivity of TMDC-based membranes. Importantly, the capillary width of TMDCs is usually <10 Å, which hinders the intercalation and transport of hydrated salt ions. In contrast, nanochannels, cavities, and gaps formed during membrane manufacturing could, however, increase the transport pathways of ions/molecules, which reduces the selectivity of membranes.[130]

From this perspective, two types of strategies enable the improvement of the sieving performance of TMDC-based membranes: pore engineering and nanochannel engineering (e.g., molecule modification and ion modification). Pore engineering creates suitable pores on the surface of TMDC nanosheets. In this way, porous TMDC nanosheets can be obtained together with intrinsic nanochannels that are beneficial for water penetration. Nanochannel engineering involves designing a water transport pathway by increasing the interlayer spacing. Thus, undesirable substances with various sizes can be selectively removed from seawater.

Nanochannel engineering
Layered structures of TMDC nanomaterials provide intrinsic nanochannels for rejecting molecules and ions to some extent. However, the size of the nanochannels is too narrow to revitalize the selectivity of TMDC-based membranes. The weak interactions, particularly the van der Waals force between TMDC layers, and the surface chalcogen atoms, make TMDC nanosheets easy to functionalize. Therefore, the size of nanopores and nanochannels could be regulated by adjusting these interactions.

Recently, many researchers have utilized organic or inorganic chemical agents to tune the size and surface properties of TMDC nanochannels. Molecule modification and ion intercalation are two main strategies.
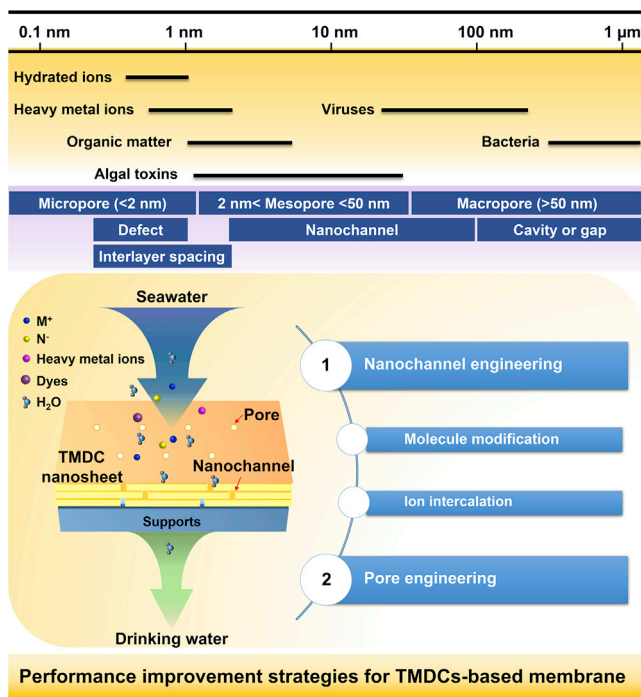
Figure 13. Schematic illustration of pore categories, the mechanism of TMDC-based membrane applied in water purification, and the corresponding performance improvement strategies

Molecule modification. Various molecules (e.g., organoidoides, polyphenols, dyes, and high-weight polymers) have been utilized to modify TMDC nanosheets. As previously noted, organic groups grafted on the surface of TMDC nanosheets could increase the size of interlayer channels due to the steric resistance effect. In 2015, Voiry et al. reported a simple method for grafting functional groups (-CH$_3$, -CH$_2$-CH$_2$-OH, and -CH$_2$-CO-NH$_2$) on TMDC monolayers (MoS$_2$, WS$_2$, and MoSe$_2$) (Figure 14A).[131] The electrophilic organic fragments derived from organoidoides could react with the electron-rich metallic 1T phase TMDC nanosheets, resulting in grafting functional groups through C-S/Se covalent bonds on the chalcogen layer. Attenuated total reflectance Fourier transform infrared (FTIR) spectroscopy (Figure 14B) and X-ray photoelectron spectroscopy (XPS) (Figure 14C) confirmed the functionalization of -CH$_3$ (Met) and -CH$_2$-CO-NH$_2$ (Fct or Acet) groups on TMDCs nanosheets by forming a C-S bond. In another work of Voiry and co-workers, ^{13}C cross-polarization magic-angle spinning nuclear magnetic resonance further proved the existence of functionalization groups (Figure 14D).[118] The X-ray diffraction (XRD) pattern (Figure 14E) and high-resolution TEM images (Figure 14F) showed that the interlayer spacing of functionalized MoS$_2$ was significantly increased. Contact angle measurements proved that grafting -CH$_3$ functional groups can increase the hydrophobicity of MoS$_2$ membranes (Figure 14G). Compared with the non-functionalized MoS$_2$ membrane, the functionalized MoS$_2$ membrane exhibited higher water permeance and increased NaCl rejection (Figure 14H). The authors postulated that small, hydrophobic functional groups play a crucial role in enhancing water flow. This study paves the way for the development of TMDC-based membranes with tunable sieving behavior.

Following the same group's grafting function strategy, acetate and amide groups were grafted on chemically exfoliated MoS$_2$ membranes using iodoacetic acid and
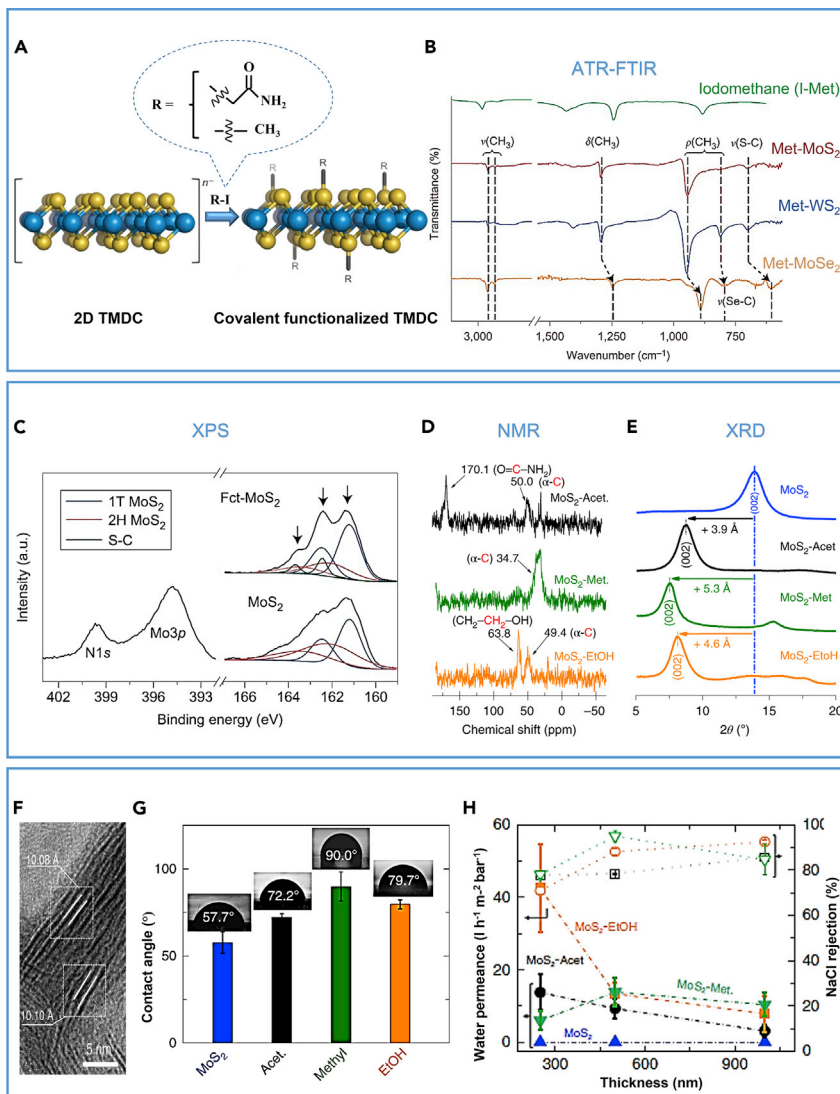
Figure 14. The strategies of TMDC-based membranes via molecule modification by grafting different functional groups

(A and B) (A) Schematic illustration of TMDC functionalized with organoiodide chemicals (R-I);
(B) attenuated total reflectance FTIR spectra of methyl-functionalized TMDCs.
(C) XPS spectra of functionalized MoS_2.[131] Copyright 2015, Springer Nature.
(D) The cross-polarization magic angle spinning nuclear magnetic resonance (NMR) spectra for different covalently functionalized MoS_2 nanosheets.
(E) XRD patterns of pristine MoS_2 membrane and functionalized MoS_2 membranes.
(F) HR-TEM image of MoS_2 nanosheets functionalized with acetamide groups.
(G) Contact angle measurements for pristine MoS_2 and functionalized MoS_2 membranes.
(H) Water permeance and NaCl rejection rate measured from MoS_2 and functionalized MoS_2 membranes.[118] Copyright 2019, Springer Nature.

2-iodoacetamide precursors.[132] These functional groups act as permanent molecular spacers to reduce the voids and impermeable regions that exist in the hydrated chemically exfoliated MoS_2 and partially dried chemically exfoliated MoS_2 membranes. Their interlayer spacing was ~1.5 times larger than that of dried chemically exfoliated MoS_2. Consequently, acetate-MoS_2 membranes achieved better ion rejection rate. Therefore, controlling the interlayer spacing and surface chemistry of nanolaminate membranes by grafting functional groups can enhance their sieving
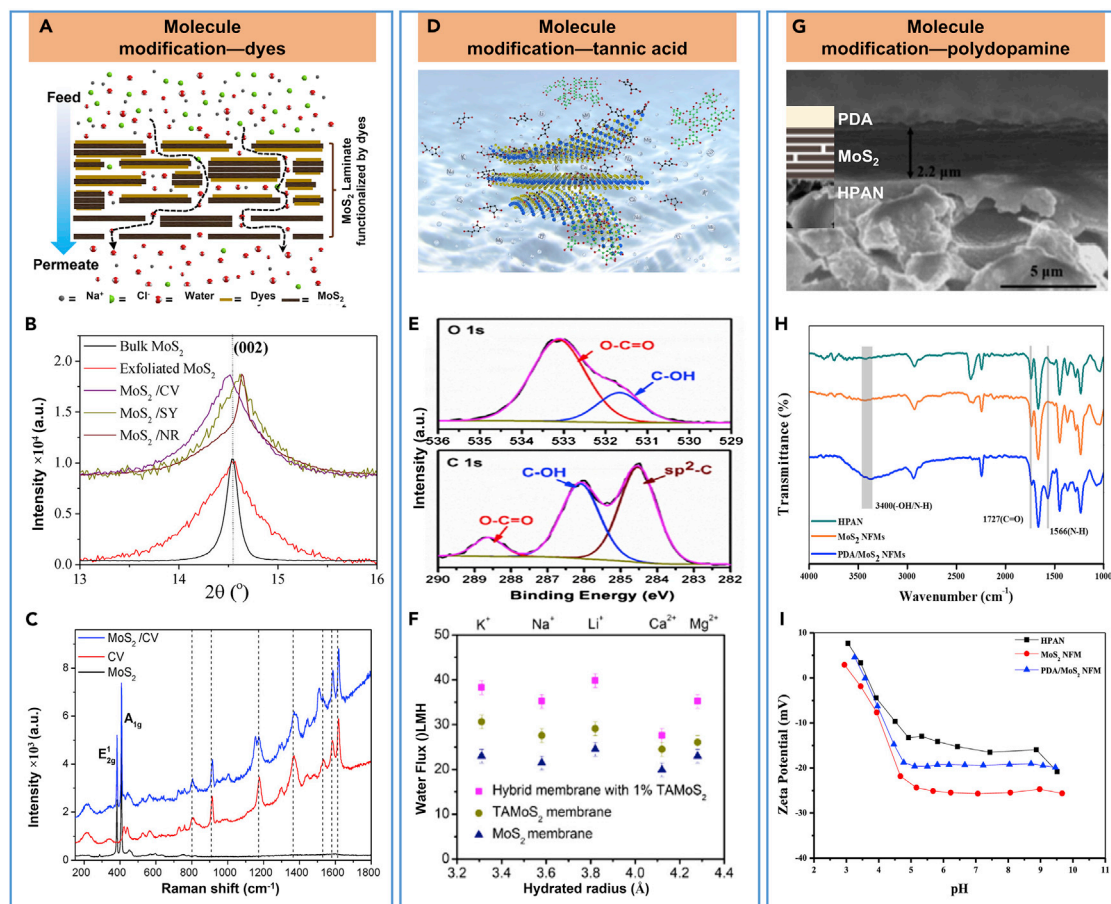
Figure 15. The improvement strategies of TMDC-based membranes via molecule modification

(A) Schematic illustration of the mixed ionic solutes that penetrate through the dye functionalized MoS_2 membrane.

(B and C) (B) XRD patterns and (C) Raman spectra of MoS_2 before and after dye molecular functionalization.[93] Copyright 2017, American Chemical Society.

(D) Schematic illustration of tannic acid-assisted exfoliation of MoS.

(E) XPS spectra of tannic acid functionalized MoS_2.

(F) Water flux performance of MoS_2 and TA-modified MoS_2 membranes.[119] Copyright 2020, Elsevier.

(G) Cross-sectional SEM image of the PDA/MoS_2 membrane.

(H) FTIR spectra and (I) Zeta-potentials of the MoS_2 membrane before and after PDA modification.[133] Copyright 2020, American Chemical Society.

performance. Thus, more functional groups could be explored to adjust the inter-layer spacing of MoS_2 and other TMDCs to improve the selectivity of TMDC-based membranes.

Dyes or high-weight polymers were usually selected for molecule modification. For example, Bissett and co-workers used three types of dyes to functionalize MoS_2 (Figure 15A).[93] XRD patterns (Figure 15B) and Raman spectra (Figure 15C) were used to confirm the existence of dye molecule functionalization. Although Bissett et al. demonstrated that dye functionalization altered the MoS_2 membrane surface charge, they did not elucidate the mechanism by which the formed nanochannels affected the ionic sieving properties of the membranes.

In addition to dyes, tannic acid (TA) was utilized to modify the MoS_2 membrane.[119,121] TA molecules interact with negatively charged sulfur atoms on the surface defects during the exfoliation process (Figure 15D).[119] XPS confirmed this

type of functionalization (Figure 15E). Consequently, TA-modified MoS_2 membrane demonstrated high water flux and high dye rejection rate, which was attributed to the cation-π interactions between TA molecules and hydrated cations (Figure 15F). Similar to TA, dopamine was also utilized to modify layer-stacked MoS_2 membranes through a polymerization process (Figure 15G).[133] FTIR spectra (Figure 15H) confirmed the existence of -OH/N-H bonds in functionalized MoS_2 membranes. Zeta potential measurement (Figure 15I) proved that electronegativity of modified membrane was increased compared with the pristine membrane. Since polydopamine possessed abundant hydroxyl and amide functional groups, it improved the MoS_2 surface hydrophilicity and antifouling properties of MoS_2 nanosheets, resulting in high water permeance (135.3 L m^{-2} h^{-1} bar^{-1}) and long-term stability (~168 h operation).

To date, various additional organic molecules, such as sucrose,[115] tetraheptylammonium bromide,[134,135] mercaptopropionic acid,[136,137] PEO,[138] polyglycerol,[139] and triethanolamine,[140] have been successfully explored to expand the interlayer spacing of TMDC nanosheets using a molecule modification strategy. Consequently, using this strategy effectively enhanced the desired water desalination and purification performance by altering the surface properties of TMDC nanosheets. However, the relationship between the structure and purification performance of modified TMDCs has not been explored; thus, further studies are required for investigation.

Ion intercalation. The ion intercalation strategy has been explored to control the interlayer distance of TMDC layers. Cations (e.g., K^+, Na^+, Li^+, or Mg^{2+}) were successfully intercalated into MoS_2 nanosheets; then, its interlayer width was increased from the original value of ~3 Å to as large as 8.48 Å.[141] This modification process involves immersing a water-saturated MoS_2 membrane into specific salt solutions (usually chlorides), which is similar to the organoiodide covalent functionalization method; however, the former requires a considerably shorter reaction time (only 0.5 h).

Adjusting the stacking behavior of TMDC nanosheets is usually helpful for improving the rejection rate of organic matter or algal toxins. Through a medium-speed vacuum filtration process (pressure, 0.5 bar), MoS_2 fragments were loosely stacked together forming a lamellar membrane with narrow gaps and large cavities.[112] These gaps, made by contacting the edges of fragments and cavities, exist among stacked fragments and provide unobstructed nanochannels for the transport of molecules. However, the loosely stacked MoS_2 membranes could only reject dye molecules larger than 1.9 nm. Nevertheless, it is reasonable to expect that regulating stacking forms of nanosheets will result in better selectivity of TMDC-based membranes.

Pore engineering
Engineering pores is another valid strategy for improving the selectivity of TMDC-based membranes. Typically, pore engineering involves regulating the shape, size, density, and location of pores in TMDC nanosheets. Theoretically, MoS_2 membranes with single-layer structure-derived pores, possessing Mo atoms located at the pore center and S atoms at the edge, exhibited both high water flux and high arsenic rejection.[142] Experimentally, probe sonication and chemical etching have been utilized to generate pores with different sizes and disordered locations.

Typically, the probe sonication method can create nanopores because of acoustic cavitation phenomena (i.e., cavitation effect). It induces high-speed jets and intense
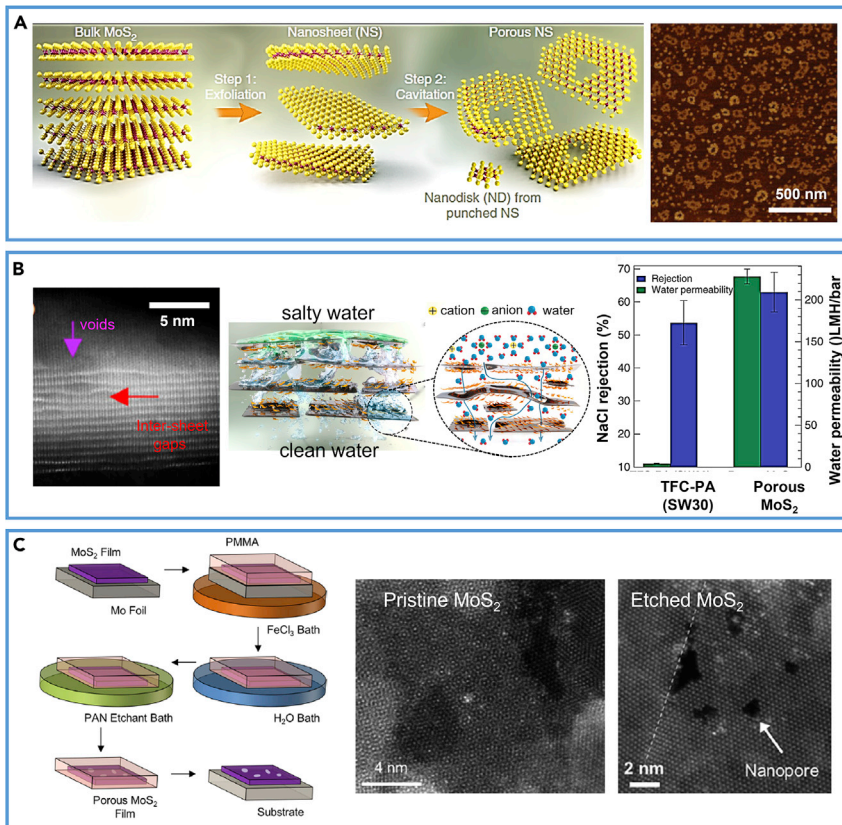
Figure 16. The improvement strategies of TMDC-based membranes via pore engineering
(A) Schematic illustration of probe sonication method for preparing porous MoS_2 nanodisks and the corresponding AFM image.
(B) A HAADF-STEM image of the porous MoS_2 membrane. Graphical depiction of sub-nanometer water pathways and membrane' desalination performance.[51] Copyright 2014, Springer Nature.
(C) Schematic illustration of the chemical etching method for fabricating nanoporous MoS_2 membrane and its HAADF-STEM image before and after etching.[143] Copyright 2019, American Chemical Society.

shock waves to create nanopores on the surface of the nanosheets or reduce the size of the nanosheets. Based on this, Wanunu and co-workers prepared porous MoS_2 nanodisks by a two-step sonicating method (Figure 16A).[51] Owing to the cavitation effect, the MoS_2 nanodisks possessed a pore size of 32 ± 8 nm and sheet size of 163 ± 20 nm. Meanwhile, voids and gaps were formed by porous laminated nanodisks providing abundant sub-nanometer pathways for the transportation of water molecules (Figure 16B). The orderly stacked laminated sheets exhibited high water flux and ion selectivity.

In addition, Drndić and co-workers reported that randomly distributed pores were created in large areas on MoS_2 membranes by a chemical etching method.[143] As shown in Figure 16C, after the MoS_2 film was separated from the molybdenum foil substrate, an industry-standard PAN etchant was added to enlarge the intrinsic defect sites within the polycrystalline MoS_2. The PAN etchant expanded defect sites primarily located at grain boundaries, particularly transition metal vacancies, and then joined into larger nanopores. However, from the perspective of the desalination membrane, the etched nanopores are too large to reject ions and small molecules. Although the electron-beam sculpting method is popular for creating

atomic-scale nanopores in MoS$_2$ nanosheets,[54,144] the yield and quality of nanosheets are two bottlenecks when manufacturing semipermeable membranes. Thus, the precise control of the pore size in TMDC nanosheets needs to be further investigated.

In addition to shape and size, the density of pores on the nanosheets significantly affects the permeability and selectivity of the membranes.[142] However, to date, no experimental research regarding this topic has been reported. Pore engineering of thin TMDC nanosheets is in its nascent stages. Compared with pore density or location control, pore size and shape can be easily adjusted to some extent.

Overall, engineered nanopores on the nanosheets and modified nanochannels between laminates are promising strategies in the field of water purification. For porous TMDC nanosheets, generating pores with various shapes, sizes, densities, and locations is an effective way to enhance the performance of TMDC-based membranes. For non-porous TMDC nanosheets, increasing the interlayer spacing of nanosheets by grafting functional groups or intercalating molecule/ion is an essential approach to strengthen the selectivity of TMDC-based membranes. In addition, simultaneously integrating suitable pores and nanochannels into TMDC layers could improve the sieving performance of TMDC-based membranes. Additional efforts are required to break the trade-off between membrane selectivity and permeability.

PROGRESS OF THEORETICAL RESEARCH

Theoretical research is necessary for the development of TMDC nanomaterials used as water purification and desalination membranes. MD simulations and first-principles density functional theory calculations are two regular methods for verifying the structure-activity relationship of TMDC-based membranes for water desalination.[145–148] Typically, MD simulations were performed in pressure-driven filtration techniques using the LAMMPS and GROMACS program packages. During the simulation, the external pressure was precisely controlled using a fluctuating wall method. Driven by pressure gradients, water molecules and salt ions percolate through the TMDC-based membrane; thus, their transport behavior can be simulated and analyzed.

The effect of pore chemistry and pore geometry on water permeance are the focus of theoretical studies. In 2015, Aluru and co-workers reported the first theoretical study on TMDC-based membranes for water purification.[146] The simulation results showed that, compared with S-only pores and mixed pores, Mo-only pores enabled MoS$_2$ membranes with higher water flux (almost two to five orders of magnitude). This is because the Mo-only pores possessed hourglass shapes and suitable sizes ranging from 0.45 to 0.77 nm, thereby facilitating rapid water permeation. In another study, Fan and co-workers investigated the effect of pore size (e.g., P$_0$, P$_1$, P$_2$, and P$_3$) on salt rejection and water permeance using all-atom MD simulations (Figure 17A).[149] They found that the MoS$_2$ membrane with P$_1$ (0.74 nm) pores enables the most efficient salt rejection ($\sim$100%) and considerable permeation of water molecules (Figures 17B and 17C). They also postulated that the water molecules connected with single-chain hydrogen bonds on both sides of the MoS$_2$ membrane facilitated the transmembrane movement of water molecules.

Similarly, Zhou and co-workers exerted tensile strain on a monolayer MoS$_2$ membrane in MD simulations to open the pores through cross-sectional expansion (Figure 17D).[150] They found that the threshold of strain level that changed the pores
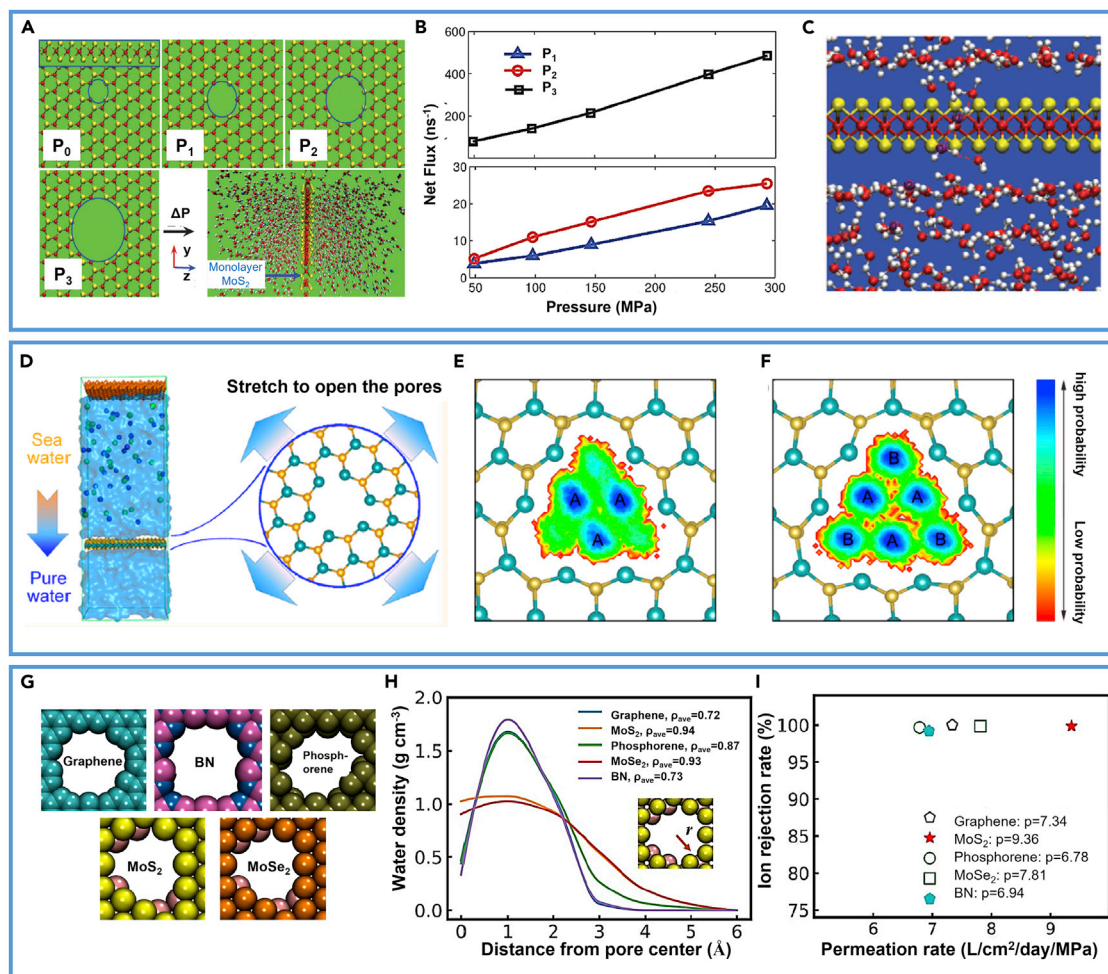
Figure 17. The theoretical studies of TMDC-based membranes via pore engineering

(A) Four types of nanopores (e.g., 0.53 [P_0], 0.74 [P_1], 0.98 [P_2], and 1.35 [P_3] nm) on the MoS_2 membrane and its selected simulation model.

(B and C) Net water flux as a function of pressure for (B) different MoS_2 membrane pores and (C) the corresponding snapshot.[149] Copyright 2016, Royal Chemical Society.

(D–F) (D) Schematic illustration of the desalination model. Water flux projected onto the cross-section of the MoS_2 nanopore when placed under strain levels of (E) 9% and (F) 12%.[150] Copyright 2016, American Chemical Society.

(G) Snapshots of ∼50 Å^2 nanopores drilled in five different membrane materials.

(H) Water density as a function of the distance from the pore center for different membranes.

(I) Water desalination performance of different membrane materials.[151] Copyright 2020, American Chemical Society.

from "closed" state to "open" state for water passage was at least 6%. Further strengthening the tensile strain could increase the number of water flow channels (the areas marked with "A" and "B" in Figures 17E and 17F). From another perspective, pores in the "open" state have enlarged pore sizes. This theoretical study provides strong support for further investigation of fabricating porous MoS_2 membranes. In another study, researchers proposed an optimized theoretical model for artificial nanopores to elucidate the relationship between high-permeability performance and pore structure, providing a guideline to design and optimize the TMDC-based desalination membranes.[152]

Recently, Barati Farimani and co-workers demonstrated that, compared with other 2D monolayer membranes, such as graphene, phosphorene, boron nitride, and $MoSe_2$, MoS_2 exhibited the highest desalination performance owing to its low

energy consumption (Figures 17G–17I).[151] They also determined the fundamental physics behind such high performance, which is the combined effect of the water structure and membrane dynamics factors. This study provides insight into understanding the mechanism of MoS$_2$ membranes for water desalination. In another recent theoretical study, Barbosa and co-workers proposed that, compared with the water model employed in previous studies, the salt model had a greater effect on the water permeability and salt rejection, especially for narrow pores with a diameter of 0.74 nm.[153] This new distinct mechanism of the salt model helps to understand the behavior of water desalination at greater depths.

To date, most theoretical studies on the effect of nanochannels for water desalination have demonstrated that the confined water molecules can form a unique surface state of nanochannels, which is beneficial for high water flux. For example, Wang et al. observed that confined water molecules built a well-aligned, rhombus-shaped monolayer water network in hydrated MoS$_2$ layers (Figure 18A).[94] This hydrated MoS$_2$ membrane possessed a nanochannel with an increased interlayer spacing of 1.2 nm, which was twice as large as that of a dry MoS$_2$ membrane (0.62 nm). In another study, Onofrio and co-workers theoretically demonstrated that water molecules are usually pinned on top of sulfur atoms (Figure 18B).[118] This means that the sulfur atoms provide a template for the water structure, which is presented as a "pinning point." They also found that grafted hydrophobic methyl groups occupied some pinning point, thus enhancing the velocity of water molecules. Moreover, a theoretical study reported that functional groups prefer bonding with the 1T phase of MoS$_2$ because of its metallic character and partly filled Mo 4d states.[154]

Recently, Jung and co-workers suggested that confined water molecules built planar multilayered water structures (with up to four layers) in nanochannel areas between two MoS$_2$ nanosheets (Figure 18C).[155] Thus, the interlayer spacing of nanochannels expanded, varying from 0.55 to 1.3 nm. More recently, Oviroh et al. reported that the salt rejection of MoS$_2$ membrane increased with the layer number of the multilayer MoS$_2$, following the trend of trilayer > bilayer > monolayer (Figure 18D), but simultaneously water permeability was sacrificed.[156]

Although the relationship between water permeance and nanochannel structure has been studied, very few reports have been published on the effect of the nanochannel on selectivity performance. Only one study reported that the selectivity of the MoS$_2$ lamellar structure was reduced by framework defects in the Monte Carlo simulation.[113] Before this, the influence of such framework defects on the desalination performance of graphene membranes was investigated using the same simulation method.[157] These works elucidate the discrepancy between the theoretical calculations and experimental scenarios, promoting the development of theoretical calculations for membrane desalination.

Overall, computational studies suggest that TMDC-based nanomaterials have obvious advantages in the field of membrane-based water purification. The geometry and surface chemistry state of pores and nanochannels are two important factors that determine the water permeance and salt rejection performance. For example, Mo-only or hour-glass-shaped pores with a size of ∼0.74 nm are identical for penetrating water molecules. Nanochannels of MoS$_2$ membranes modified with hydrophobic functional groups possess higher water molecule velocity than the original MoS$_2$ membrane. Furthermore, confined water molecules in nanochannels could form single- or multilayer network structure, thus favoring water permeance. Nevertheless, the transport mechanism of water and other molecules and ions in
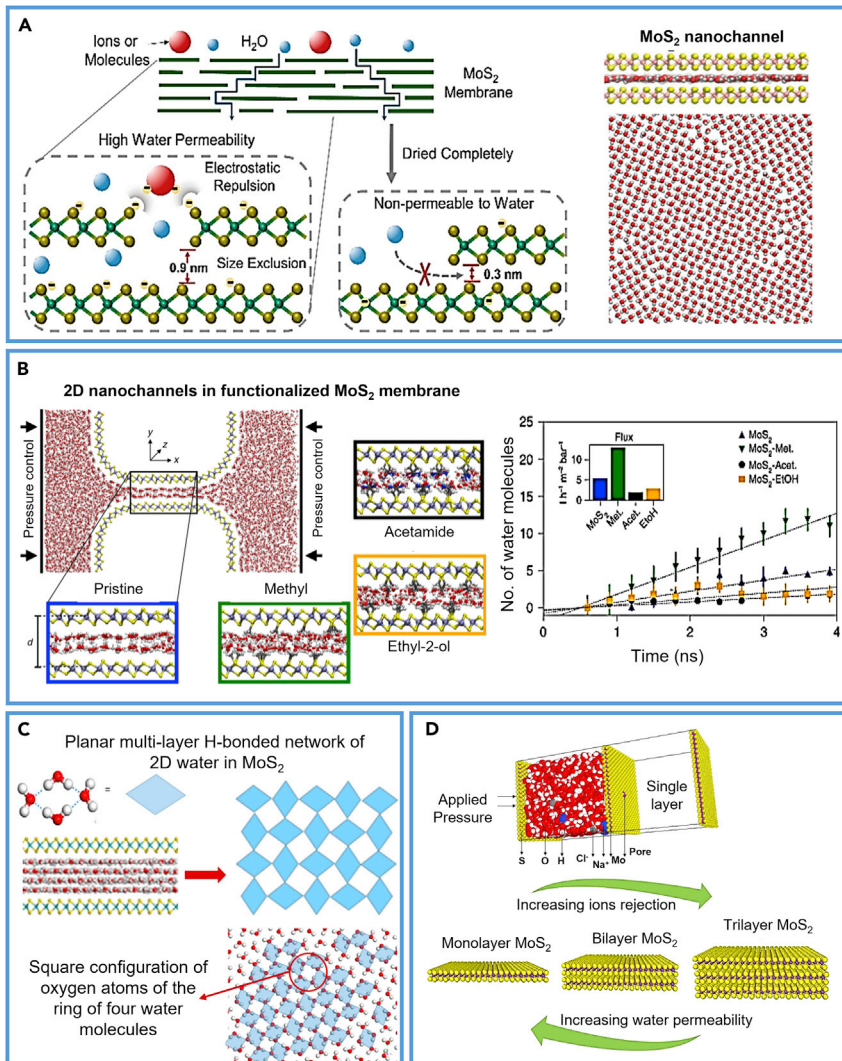
Figure 18. The theoretical studies of TMDC-based membranes via nanochannel engineering
(A) Schematic illustration of the proposed mechanism and monolayer water network in the MoS$_2$ membrane.[94] Copyright 2017, American Chemical Society.
(B) Snapshot of a typical atomistic model; the number of water molecules crossing the midpoint of the nanochannel as a function of simulation time.[118] Copyright 2019, Springer Nature.
(C) Schematic illustration of planar multilayer H-bonded network of 2D water in the MoS$_2$ membrane desalination model.[155] Copyright 2017, American Chemical Society.
(D) Schematic illustration of the single-layer, bilayer and trilayer MoS$_2$ RO systems.[156] Copyright 2021, American Chemical Society.

the MoS$_2$ membrane is still unclear. Consequently, limited by the development of computational modeling, the gap between the theoretical calculation results and experimental outcomes cannot be ignored.

CONCLUSION AND OUTLOOK

In this review, we focus on TMDC nanomaterials for water purification and desalination. In "Understanding water desalination," we introduce the basic background of water desalination and clarify the performance evaluation criteria and influencing factors. This crucial information allows new researchers to outline water desalination

processes. In the main body of the review, we highlight all the synthesis methods for 2D layered TMDC nanomaterials and TMDC-based functional membrane engineering processes. Most importantly, several novel TMDC-based functional membranes for water desalination are systematically summarized. Furthermore, modification approaches to improve membrane desalination performance are discussed in detail. Finally, theoretical investigation of TMDC membranes is reviewed. This helps researchers to understand the relationship between desalination performance and membrane structure, the mechanism of water penetration, and ion/molecule rejection, and thus provides a guideline for designing optimal TMDC-based functional membranes.

Although 2D TMDC nanomaterials possess many advantages that make them potential candidates for water desalination, this review demonstrates that TMDC-based functional membranes are still in the nascent stages. Continuous studies are required to explore various 2D TMDC nanomaterials or further improve the performance of reported TMDC-based membranes. However, several issues need to be addressed:

(1) Control of nanosheets and membranes

Most of the present studies focused on multilayer MoS_2 nanosheets with low aspect ratios, and very few reports can be found on single-layer TMDC nanosheets. The thickness of the obtained TMDC-based membranes was too thick to acquire high water flux. More importantly, the effect of membrane surface roughness on desalination performance has not yet been investigated, which is crucial for developing desalination membranes with high fouling resistance.

(2) Nanopore and nanochannel engineering

Nanopore and nanochannel structures contribute to enhancing the selectivity of TMDC-based membranes. Although chemical etching and sonication methods have been used to generate nanopores on 2D TMDC nanosheets, precise control of the size, shape, and surface chemistry state of the created pores remains difficult, even in the laboratory. Effective utilization of nanochannels between layered TMDC nanosheets has not been successful. Moreover, additional research efforts are required to control the size and chemistry state of nanochannels to obtain desalination membranes with high permeability and selectivity.

(3) Desalination mechanism

The current theoretical research mainly focuses on simulating the confined water molecules in TMDC nanochannels or the relationship between water flux and pore structure by using MD simulations. Due to the limited computational modeling methods, a gap between simulation results and experimental outcomes still exists. The sieving mechanism of TMDC-based membranes related to pores and nanochannels remains unclear. Thus, more computational models and simulations need to be explored to elucidate the mass transport in the process of water desalination.

(4) Performance evaluation

To date, most researchers have characterized the water desalination performance in the laboratory under a condition of simulated desalination brine with single or just several components, which is not operated at practical working conditions. Usually, the lab-scale performance at idealized conditions can be overestimated. Therefore, a comprehensive investigation on practical conditions is also needed. Moreover, standard and quantitative characterization of TMDC-based membranes for water desalination should be established for the development of commercial products.

AUTHOR CONTRIBUTIONS

Z.Z. proposed the topic of the review. Z.Z., R.W., and Z.Q. supervised the project. H.P. and Z.Z. drafted and envisioned the manuscript. All authors contributed to the review and editing of the manuscript.

DECLARATION OF INTERESTS

The authors declare no competing interests.

REFERENCES

1. Sharma, S. (2017). Water Challenges of an Urbanizing World (INTECH). Chapter 7.

2. Shannon, M.A., Bohn, P.W., Elimelech, M., Georgiadis, J.G., Mariñas, B.J., and Mayes, A.M. (2008). Science and technology for water purification in the coming decades. Nature 452, 301–310.

3. WHO; UNICEF (2017). Progress on drinking water, sanitation and hygiene: 2017 update and SDG baselines. World Health Organization 1, 3.

4. Wang, Z., Horseman, T., Straub, A.P., Yip, N.Y., Li, D., Elimelech, M., and Lin, S. (2019). Pathways and challenges for efficient solar thermal desalination. Sci. Adv. 5, eaax0763.

5. Tian, S., Huang, Z., Tan, J., Cui, X., Xiao, Y., Wan, Y., Li, X., Zhao, Q., Li, S., and Lee, C.-S. (2020). Manipulating interfacial charge-transfer absorption of cocrystal absorber for efficient solar seawater desalination and water purification. ACS Energy Lett. 5, 2698–2705.

6. Liu, T., Serrano, J., Elliott, J., Yang, X., Cathcart, W., Wang, Z., He, Z., and Liu, G. (2020). Exceptional capacitive deionization rate and capacity by block copolymer–based porous carbon fibers. Sci. Adv. 6, eaaz0906.

7. Zhang, X., Zuo, K., Zhang, X., Zhang, C., and Liang, P. (2020). Selective ion separation by capacitive deionization (CDI) based technologies: a state-of-the-art review. Environ. Sci. Water Res. Technol. 6, 243–257.

8. Patel, S.K., Ritt, C.L., Deshmukh, A., Wang, Z., Qin, M., Epsztein, R., and Elimelech, M. (2020). The relative insignificance of advanced materials in enhancing the energy efficiency of desalination technologies. Energy Environ. Sci. 13, 1694–1710.

9. Qasim, M., Badrelzaman, M., Darwish, N.N., Darwish, N.A., and Hilal, N. (2019). Reverse osmosis desalination: a state-of-the-art review. Desalination 459, 59–104.

10. Zhang, Z., Li, S., Mi, B., Wang, J., and Ding, J. (2020). Surface slip on rotating graphene membrane enables the temporal selectivity that breaks the permeability-selectivity trade-off. Sci. Adv. 6, eaba9471.

11. Liu, C., Wang, W., Yang, B., Xiao, K., and Zhao, H. (2021). Separation, anti-fouling, and chlorine resistance of the polyamide reverse osmosis membrane: from mechanisms to mitigation strategies. Water Res. 195, 116976.

12. Surwade, S.P., Smirnov, S.N., Vlassiouk, I.V., Unocic, R.R., Veith, G.M., Dai, S., and Mahurin, S.M. (2015). Water desalination using nanoporous single-layer graphene. Nat. Nanotechnol. 10, 459–464.

13. Huang, H.H., Joshi, R.K., De Silva, K.K.H., Badam, R., and Yoshimura, M. (2019). Fabrication of reduced graphene oxide membranes for water desalination. J. Membr. Sci. 572, 12–19.

14. Ding, L., Wei, Y., Wang, Y., Chen, H., Caro, J., and Wang, H. (2017). A two-dimensional lamellar membrane: MXene nanosheet stacks. Angew Chem. Int. Ed. Engl. 56, 1825–1829.

15. Graf, M., Lihter, M., Thakur, M., Georgiou, V., Topolancik, J., Ilic, B.R., Liu, K., Feng, J., Astier, Y., and Radenovic, A. (2019). Fabrication and practical applications of molybdenum disulfide nanopores. Nat. Protoc. 14, 1130–1168.

16. Zandiatashbar, A., Lee, G.H., An, S.J., Lee, S., Mathew, N., Terrones, M., Hayashi, T., Picu, C.R., Hone, J., and Koratkar, N. (2014). Effect of defects on the intrinsic strength and stiffness of graphene. Nat. Commun. 5, 3186.

17. Perreault, F., de Faria, A.F., Nejati, S., and Elimelech, M. (2015). Antimicrobial properties of graphene oxide nanosheets: why size matters. ACS Nano 9, 7226–7236.

18. Abraham, J., Vasu, K.S., Williams, C.D., Gopinadhan, K., Su, Y., Cherian, C.T., Dix, J., Prestat, E., Haigh, S.J., Grigorieva, I.V., et al. (2017). Tunable sieving of ions using graphene oxide membranes. Nat. Nanotechnol. 12, 546–550.

19. Wang, X., Li, Q., Zhang, J., Huang, H., Wu, S., and Yang, Y. (2020). Novel thin-film reverse osmosis membrane with MXene Ti_3C_2T embedded in polyamide to enhance the water flux, anti-fouling and chlorine resistance for water desalination. J. Membr. Sci. 603, 118036.

20. Lu, Z., Wei, Y., Deng, J., Ding, L., Li, Z.K., and Wang, H. (2019). Self-crosslinked MXene $(Ti_3C_2T_x)$ membranes with good antiswelling property for monovalent metal ion exclusion. ACS Nano 13, 10535–10544.

21. Adigilli, H.K., Pandey, A.K., and Joardar, J. (2019). 2D-nanolayered tungsten and molybdenum disulfides: structure, properties, synthesis, and processing for strategic applications. In Handbook of advanced ceramics and composites: defense, security, aerospace and energy applications, Y. Mahajan and J. Roy, eds. (Springer International Publishing), pp. 1–47.

22. Yadav, V., Rajput, A., and Kulshrestha, V. (2020). Sulfonated poly(ether sulfone) based sulfonated molybdenum sulfide composite membranes and their applications in salt removal and alkali recovery. J. Membr. Sci. 603, 118043.

23. Zhang, H., Chhowalla, M., and Liu, Z. (2018). 2D nanomaterials: graphene and transition metal dichalcogenides. Chem. Soc. Rev. 47, 3015–3017.

24. He, Y., He, Q., Wang, L., Zhu, C., Golani, P., Handoko, A.D., Yu, X., Gao, C., Ding, M., Wang, X., et al. (2019). Self-gating in semiconductor electrocatalysis. Nat. Mater. 18, 1098–1104.

25. Yang, S., Jiang, Q., and Zhang, K. (2020). Few-layers 2D O-MoS$_2$ TFN nanofiltration membranes for future desalination. J. Membr. Sci. 604, 118052.

26. Zhu, J., Hou, J., Uliana, A., Zhang, Y., Tian, M., and Van der Bruggen, B. (2018). The rapid emergence of two-dimensional nanomaterials for high-performance separation membranes. J. Mater. Chem. 6, 3773–3792.

27. Gravelle, S., Joly, L., Detcheverry, F., Ybert, C., Cottin-Bizonne, C., and Bocquet, L. (2013). Optimizing water permeability through the hourglass shape of aquaporins. Proc. Natl. Acad. Sci. USA 110, 16367–16372.

28. Azamat, J., and Khataee, A. (2017). Improving the performance of heavy metal separation from water using MoS$_2$ membrane: molecular dynamics simulation. Comput. Mater. Sci. 137, 201–207.

29. Presolski, S., and Pumera, M. (2016). Covalent functionalization of MoS$_2$. Mater. Today 19, 140–145.

30. Bertolazzi, S., Gobbi, M., Zhao, Y., Backes, C., and Samorì, P. (2018). Molecular chemistry approaches for tuning the properties of two-dimensional transition metal dichalcogenides. Chem. Soc. Rev. 47, 6845–6888.

31. Kumar, P., Roy, S., Sarkar, A., and Jaiswal, A. (2021). Reusable MoS$_2$-modified antibacterial fabrics with photothermal disinfection properties for repurposing of personal protective masks. ACS Appl. Mater. Interfaces 13, 12912–12927.

32. Li, Y., Yang, S., Zhang, K., and Van der Bruggen, B. (2019). Thin film nanocomposite reverse osmosis membrane modified by two dimensional laminar MoS$_2$ with improved desalination performance and fouling-resistant characteristics. Desalination 454, 48–58.

33. Dahanayaka, M., Liu, B., Srikanth, N., and Zhou, K. (2020). Ionised graphene oxide membranes for seawater desalination. Desalination 496, 114637.

34. Qiu, H., Xue, M., Shen, C., Zhang, Z., and Guo, W. (2019). Graphynes for water desalination and gas separation. Adv. Mater. 31, 1803772.

35. Karahan, H.E., Goh, K., Zhang, C.J., Yang, E., Yıldırım, C., Chuah, C.Y., Ahunbay, M.G., Lee, J., Tantekin-Ersolmaz, Ş.B., Chen, Y., and Bae, T.H. (2020). MXene materials for designing advanced separation membranes. Adv. Mater. 32, 1906697.

36. Malik, R. (2018). Maxing out water desalination with MXenes. Joule 2, 591–593.

37. Memon, F.H., Rehman, F., Lee, J., Soomro, F., Iqbal, M., Khan, S.M., Ali, A., Thebo, K.H., and Choi, K.H. (2022). Transition metal dichalcogenide-based membranes for water desalination, gas separation, and energy storage. Separation & Purification Reviews. Separ. Purif. Rev. 1–15.

38. Yang, Z., Long, L., Wu, C., and Tang, C.Y. (2021). High permeance or high selectivity? Optimization of system-scale nanofiltration performance constrained by the upper bound. ACS EST. Eng. 2, 377–390.

39. Bolisetty, S., Peydayesh, M., and Mezzenga, R. (2019). Sustainable technologies for water purification from heavy metals: review and analysis. Chem. Soc. Rev. 48, 463–487.

40. Nie, L., Chuah, C.Y., Bae, T., and Lee, J. (2021). Graphene-based advanced membrane applications in organic solvent nanofiltration. Adv. Funct. Mater. 31, 2006949.

41. Zhang, H., Wu, M.S., Zhou, K., and Law, A.W.-K. (2019). Molecular insights into the composition-structure-property relationships of polyamide thin films for reverse osmosis desalination. Environ. Sci. Technol. 53, 6374–6382.

42. Jiang, Z., Karan, S., and Livingston, A.G. (2018). Thin films: water transport through ultrathin polyamide nanofilms used for reverse osmosis. Adv. Mater. 30, 1870107.

43. Suwaileh, W., Pathak, N., Shon, H., and Hilal, N. (2020). Forward osmosis membranes and processes: a comprehensive review of research trends and future outlook. Desalination 485, 114455.

44. Peng, L.E., Yao, Z., Chen, J., Guo, H., and Tang, C.Y. (2020). Highly selective separation and resource recovery using forward osmosis membrane assembled by polyphenol network. J. Membr. Sci. 611, 118305.

45. Shi, L., Rossi, R., Son, M., Hall, D.M., Hickner, M.A., Gorski, C.A., and Logan, B.E. (2020). Using reverse osmosis membranes to control ion transport during water electrolysis. Energy Environ. Sci. 13, 3138–3148.

46. Zhao, D.L., Japip, S., Zhang, Y., Weber, M., Maletzko, C., and Chung, T.S. (2020). Emerging thin-film nanocomposite (TFN) membranes for reverse osmosis: a review. Water Res. 173, 115557.

47. Ghoufi, A., Draževi\'c, E., and Szymczyk, A. (2017). Interactions of organics within hydrated selective layer of reverse osmosis desalination membrane: a combined experimental and computational study. Environ. Sci. Technol. 51, 2714–2719.

48. Asadollahi, M., Bastani, D., and Musavi, S.A. (2017). Enhancement of surface properties and performance of reverse osmosis membranes after surface modification: a review. Desalination 420, 330–383.

49. Arshad, F., Aubry, C., Ravaux, F., and Zou, L. (2021). 2D MoS$_2$ nanoplatelets for fouling resistant membrane surface. J. Colloid Interface Sci. 590, 415–423.

50. Culp, T.E., Khara, B., Brickey, K.P., Geitner, M., Zimudzi, T.J., Wilbur, J.D., Jons, S.D., Roy, A., Paul, M., Ganapathysubramanian, B., et al. (2021). Nanoscale control of internal inhomogeneity enhances water transport in desalination membranes. Science 371, 72–75.

51. Sapkota, B., Liang, W., VahidMohammadi, A., Karnik, R., Noy, A., and Wanunu, M. (2020). High permeability sub-nanometre sieve composite MoS$_2$ membranes. Nat. Commun. 11, 3705.

52. Feng, J., Liu, K., Graf, M., Lihter, M., Bulushev, R.D., Dumcenco, D., Alexander, D.T.L., Krasnozhon, D., Vuletic, T., Kis, A., and Radenovic, A. (2015). Electrochemical reaction in single layer MoS$_2$: nanopores opened atom by atom. Nano Lett. 15, 3431–3438.

53. Feng, J., Graf, M., Liu, K., Ovchinnikov, D., Dumcenco, D., Heiranian, M., Nandigana, V., Aluru, N.R., Kis, A., and Radenovic, A. (2016). Single-layer MoS$_2$ nanopores as nanopower generators. Nature 536, 197–200.

54. Liu, K., Feng, J., Kis, A., and Radenovic, A. (2014). Atomically thin molybdenum disulfide nanopores with high sensitivity for DNA translocation. ACS Nano 8, 2504–2511.

55. Porter, C.J., Werber, J.R., Zhong, M., Wilson, C.J., and Elimelech, M. (2020). Pathways and challenges for biomimetic desalination membranes with sub-nanometer channels. ACS Nano 14, 10894–10916.

56. Mei, L., Cao, Z., Ying, T., Yang, R., Peng, H., Wang, G., Zheng, L., Chen, Y., Tang, C.Y., Voiry, D., et al. (2022). Simultaneous electrochemical exfoliation and covalent functionalization of MoS$_2$ membrane for ion sieving. Adv. Mater. 34, 2201416.

57. Coleman, J.N., Lotya, M., O'Neill, A., Bergin, S.D., King, P.J., Khan, U., Young, K., Gaucher, A., De, S., Smith, R.J., et al. (2011). Two-dimensional nanosheets produced by liquid exfoliation of layered materials. Science 331, 568–571.

58. Kwak, I.H., Kwon, I.S., Abbas, H.G., Jung, G., Lee, Y., Park, J., and Kang, H.S. (2018). Stable methylammonium-intercalated 1T'-MoS$_2$ for efficient electrocatalytic hydrogen evolution. J. Mater. Chem. 6, 5613–5617.

59. Sato, K., Noji, T., Hatakeda, T., Kawamata, T., Kato, M., and Koike, Y. (2017). New lithium- and diamines-intercalated superconductors Li$_x$(C$_2$H$_8$N$_2$)$_y$TiSe$_2$ and Li$_x$(C$_6$H$_{16}$N$_2$)$_y$TiSe$_2$. J. Physical Soc. Japan 86, 104701.

60. Nicolosi, V., Chhowalla, M., Kanatzidis, M.G., Strano, M.S., and Coleman, J.N. (2013). Liquid exfoliation of layered materials. Science 340, 1226419.

61. Manos, M.J., and Kanatzidis, M.G. (2016). Metal sulfide ion exchangers: superior sorbents for the capture of toxic and nuclear waste-related metal ions. Chem. Sci. 7, 4804–4824.

62. Yang, R., Mei, L., Zhang, Q., Fan, Y., Shin, H.S., Voiry, D., and Zeng, Z. (2022). High-yield production of mono- or few-layer transition metal dichalcogenide nanosheets by electrochemical lithium ion intercalation-based exfoliation method. Nat. Protoc. 17, 358–377.

63. Zhou, Z., Li, B., Shen, C., Wu, D., Fan, H., Zhao, J., Li, H., Zeng, Z., Luo, Z., Ma, L., and Tan, C. (2020). Metallic 1T phase enabling MoS$_2$ nanodots as an efficient agent for photoacoustic imaging guided photothermal therapy in the near-infrared-II window. Small 16, 2004173.

64. Liu, H., Chen, B., Liao, L., Fan, P., Hai, Y., Wu, Y., Lv, G., Mei, L., Hao, H., Xing, J., and Dong, J. (2019). The influences of Mg intercalation on the structure and supercapacitive

behaviors of MoS$_2$. J. Mater. Sci. *54*, 13247–13254.

65. Zeng, Z., Yin, Z., Huang, X., Li, H., He, Q., Lu, G., Boey, F., and Zhang, H. (2011). Single-layer semiconducting nanosheets: high-yield preparation and device fabrication. Angew Chem. Int. Ed. Engl. *123*, 11289–11293.

66. Liu, N., Kim, P., Kim, J.H., Ye, J.H., Kim, S., and Lee, C.J. (2014). Large-area atomically thin MoS$_2$ nanosheets prepared using electrochemical exfoliation. ACS Nano *8*, 6902–6910.

67. O'Neill, A., Khan, U., and Coleman, J.N. (2012). Preparation of high concentration dispersions of exfoliated MoS$_2$ with increased flake size. Chem. Mater. *24*, 2414–2421.

68. Leong, S.X., Mayorga-Martinez, C.C., Sofer, Z., Luxa, J., Tan, S.M., and Pumera, M. (2017). A study of the effect of sonication time on the catalytic performance of layered WS$_2$ from various sources. Phys. Chem. Chem. Phys. *19*, 2768–2777.

69. Biccai, S., Barwich, S., Boland, D., Harvey, A., Hanlon, D., McEvoy, N., and Coleman, J.N. (2018). Exfoliation of 2D materials by high shear mixing. 2D Mater. *6*, 015008.

70. Joensen, P., Frindt, R.F., and Morrison, S. (1986). Single-layer MoS$_2$. Mater. Res. Bull. *21*, 457–461.

71. Zeng, Z., Zhang, X., Bustillo, K., Niu, K., Gammer, C., Xu, J., and Zheng, H. (2015). In situ study of lithiation and delithiation of MoS$_2$ nanosheets using electrochemical liquid cell transmission electron microscopy. Nano Lett. *15*, 5214–5220.

72. Zhang, Q., Ma, J., Mei, L., Liu, J., Li, Z., Li, J., and Zeng, Z. (2022). In situ TEM visualization of LiF nanosheet formation on the cathode-electrolyte interphase (CEI) in liquid-electrolyte lithium-ion batteries. Matter *5*, 1235–1250.

73. Zhang, Q., Mei, L., Cao, X., Tang, Y., and Zeng, Z. (2020). Intercalation and exfoliation chemistry of transition metal dichalcogenides. J. Mater. Chem. *8*, 15417–15444.

74. Wang, C., Jiang, J., Ruan, Y., Ao, X., Ostrikov, K., Zhang, W., Lu, J., and Li, Y.Y. (2017). Construction of MoO$_2$ quantum dot-graphene and MoS$_2$ nanoparticle-graphene nanoarchitectures toward ultrahigh lithium storage capability. ACS Appl. Mater. Interfaces *9*, 28441–28450.

75. Fausey, C.L., Zucker, I., Lee, D.E., Shaulsky, E., Zimmerman, J.B., and Elimelech, M. (2020). Tunable molybdenum disulfide-enabled fiber mats for high-efficiency removal of mercury from water. ACS Appl. Mater. Interfaces *12*, 18446–18456.

76. Zhu, Z., Tang, Y., Lv, Z., Wei, J., Zhang, Y., Wang, R., Zhang, W., Xia, H., Ge, M., and Chen, X. (2018). Fluoroethylene carbonate enabling a robust LiF-rich solid electrolyte interphase to enhance the stability of the MoS$_2$ anode for lithium-ion storage. Angew Chem. Int. Ed. Engl. *57*, 3656–3660.

77. Peng, H., Liu, T., Li, Y., Wei, X., Cui, X., Zhang, Y., and Xiao, P. (2018). Hierarchical MoS$_2$-Coated V$_2$O$_3$ composite nanosheet tubes as

both the cathode and anode materials for pseudocapacitors. Electrochim. Acta *277*, 218–225.

78. Ding, W., Hu, L., Dai, J., Tang, X., Wei, R., Sheng, Z., Liang, C., Shao, D., Song, W., Liu, Q., et al. (2019). Highly ambient-stable 1T-MoS$_2$ and 1T-WS$_2$ by hydrothermal synthesis under high magnetic fields. ACS Nano *13*, 1694–1702.

79. Xu, X., Zhao, R., Ai, W., Chen, B., Du, H., Wu, L., Zhang, H., Huang, W., and Yu, T. (2018). Controllable design of MoS$_2$ nanosheets anchored on nitrogen-doped graphene: toward fast sodium storage by tunable pseudocapacitance. Adv. Mater. *30*, 1800658.

80. Wang, G., Zhang, J., Yang, S., Wang, F., Zhuang, X., Müllen, K., and Feng, X. (2018). Vertically aligned MoS$_2$ nanosheets patterned on electrochemically exfoliated graphene for high-performance lithium and sodium storage. Adv. Energy Mater. *8*, 1702254.

81. Jiao, Y., Mukhopadhyay, A., Ma, Y., Yang, L., Hafez, A.M., and Zhu, H. (2018). Ion transport nanotube assembled with vertically aligned metallic MoS$_2$ for high rate lithium-ion batteries. Adv. Energy Mater. *8*, 1870071.

82. Zhang, X., Zhao, R., Wu, Q., Li, W., Shen, C., Ni, L., Yan, H., Diao, G., and Chen, M. (2017). Petal-like MoS$_2$ nanosheets space-confined in hollow mesoporous carbon spheres for enhanced lithium storage performance. ACS Nano *11*, 8429–8436.

83. Wang, Y., Kong, D., Shi, W., Liu, B., Sim, G.J., Ge, Q., and Yang, H.Y. (2016). Ice templated free-standing hierarchically WS$_2$ CNT-rGO aerogel for high-performance rechargeable lithium and sodium ion batteries. Adv. Energy Mater. *6*, 1601057.

84. Guo, B.Y., Jiang, S.D., Tang, M.J., Li, K., Sun, S., Chen, P.Y., and Zhang, S. (2019). MoS$_2$ membranes for organic solvent nanofiltration: stability and structural control. J. Phys. Chem. Lett. *10*, 4609–4617.

85. Ji, Q., Li, C., Wang, J., Niu, J., Gong, Y., Zhang, Z., Fang, Q., Zhang, Y., Shi, J., Liao, L., et al. (2017). Metallic vanadium disulfide nanosheets as a platform material for multifunctional electrode applications. Nano Lett. *17*, 4908–4916.

86. Zhang, Z., Zhao, H., Teng, Y., Chang, X., Xia, Q., Li, Z., Fang, J., Du, Z., and Świerczek, K. (2018). Carbon-sheathed MoS$_2$ nanothorns epitaxially grown on CNTs: electrochemical application for highly stable and ultrafast lithium storage. Adv. Energy Mater. *8*, 1700174.

87. Li, G., Chen, Z., Li, Y., Zhang, D., Yang, W., Liu, Y., and Cao, L. (2020). Engineering substrate interaction to improve hydrogen evolution catalysis of monolayer MoS$_2$ films beyond Pt. ACS Nano *14*, 1707–1714.

88. Shi, J., Wang, X., Zhang, S., Xiao, L., Huan, Y., Gong, Y., Zhang, Z., Li, Y., Zhou, X., Hong, M., et al. (2017). Two-dimensional metallic tantalum disulfide as a hydrogen evolution catalyst. Nat. Commun. *8*, 958.

89. Zhang, Z., Niu, J., Yang, P., Gong, Y., Ji, Q., Shi, J., Fang, Q., Jiang, S., Li, H., Zhou, X., et al. (2017). Van der Waals epitaxial growth of 2D metallic vanadium diselenide single

crystals and their extra-high electrical conductivity. Adv. Mater. *29*, 1702359.

90. Zhu, L., Huan, Y., Zhang, Z., Yang, P., Hu, J., Shi, Y., Cui, F., and Zhang, Y. (2022). Growing biomorphic transition metal dichalcogenides and their alloys toward high permeable membranes and efficient electrocatalysts applications. Energy Environ. Mater. *0*, 1–11.

91. Huan, Y., Shi, J., Zou, X., Gong, Y., Xie, C., Yang, Z., Zhang, Z., Gao, Y., Shi, Y., Li, M., et al. (2019). Scalable production of two-dimensional metallic transition metal dichalcogenide nanosheet powders using NaCl templates toward electrocatalytic applications. J. Am. Chem. Soc. *141*, 18694–18703.

92. Zhu, L., Yang, P., Huan, Y., Pan, S., Zhang, Z., Cui, F., Shi, Y., Jiang, S., Xie, C., Hong, M., et al. (2020). Scalable salt-templated directed synthesis of high-quality MoS$_2$ nanosheets powders towards energetic and environmental applications. Nano Res. *13*, 3098–3104.

93. Hirunpinyopas, W., Prestat, E., Worrall, S.D., Haigh, S.J., Dryfe, R.A.W., and Bissett, M.A. (2017). Desalination and nanofiltration through functionalized laminar MoS$_2$ membranes. ACS Nano *11*, 11082–11090.

94. Wang, Z., Tu, Q., Zheng, S., Urban, J.J., Li, S., and Mi, B. (2017). Understanding the aqueous stability and filtration capability of MoS$_2$ membranes. Nano Lett. *17*, 7289–7298.

95. Cheng, P., Chen, Y., Yan, X., Wang, Y., and Lang, W.Z. (2019). Highly stable and antibacterial two-dimensional tungsten disulfide lamellar membrane for water filtration. ChemSusChem *12*, 275–282.

96. Srimuk, P., Lee, J., Tolosa, A., Kim, C., Aslan, M., and Presser, V. (2017). Titanium disulfide: a promising low-dimensional electrode material for sodium ion intercalation for seawater desalination. Chem. Mater. *29*, 9964–9973.

97. Zhang, H.-Y., Miao, A.-J., and Jiang, M. (2013). Fabrication, characterization and electrochemistry of organic–inorganic multilayer films containing polyoxometalate and polyviologen via layer-by-layer self-assembly. Mater. Chem. Phys. *141*, 482–487.

98. Liu, G., Jiang, Z., Chen, C., Hou, L., Gao, B., Yang, H., Wu, H., Pan, F., Zhang, P., and Cao, X. (2017). Preparation of ultrathin, robust membranes through reactive layer-by-layer (LbL) assembly for pervaporation dehydration. J. Membr. Sci. *537*, 229–238.

99. Li, M.N., Sun, X.F., Wang, L., Wang, S.Y., Afzal, M.Z., Song, C., and Wang, S.G. (2018). Forward osmosis membranes modified with laminar MoS$_2$ nanosheet to improve desalination performance and antifouling properties. Desalination *436*, 107–113.

100. Kang, K., Lee, K.H., Han, Y., Gao, H., Xie, S., Muller, D.A., and Park, J. (2017). Layer-by-layer assembly of two-dimensional materials into wafer-scale heterostructures. Nature *550*, 229–233.

101. Zhang, M., Gao, J., Liu, G., Zhang, M., Liu, H., Zhou, L., Liu, Y., Zheng, X., and Jiang, Y. (2021). High-throughput zwitterion-modified MoS$_2$ membranes: preparation and

application in dye desalination. Langmuir 37, 417–427.

102. Zhang, Y., Xu, L., Walker, W.R., Tittle, C.M., Backhouse, C.J., and Pope, M.A. (2017). Langmuir films and uniform, large area, transparent coatings of chemically exfoliated MoS$_2$ single layers. J. Mater. Chem. C 5, 11275–11287.

103. Chen, J., Walker, W.R., Xu, L., Krysiak, O., She, Z., and Pope, M.A. (2020). Intrinsic capacitance of molybdenum disulfide. ACS Nano 14, 5636–5648.

104. Hussain, S.A., Dey, B., Bhattacharjee, D., and Mehta, N. (2018). Unique supramolecular assembly through Langmuir-Blodgett (LB) technique. Heliyon 4, e01038.

105. Liang, X., Wang, P., Wang, J., Zhang, Y., Wu, W., Liu, J., and Van der Bruggen, B. (2019). Zwitterionic functionalized MoS$_2$ nanosheets for a novel composite membrane with effective salt/dye separation performance. J. Membr. Sci. 573, 270–279.

106. Wang, X., Xiao, Q., Wu, C., Li, P., and Xia, S. (2021). Fabrication of nanofiltration membrane on MoS$_2$ modified PVDF substrate for excellent permeability, salt rejection, and structural stability. Chem. Eng. J. 416, 129154.

107. Yang, J., Gu, Y., Lee, E., Lee, H., Park, S.H., Cho, M.H., Kim, Y.H., Kim, Y.H., and Kim, H. (2015). Wafer-scale synthesis of thickness-controllable MoS$_2$ films via solution-processing using a dimethylformamide/n-butylamine/2-aminoethanol solvent system. Nanoscale 7, 9311–9319.

108. Sun, L., Huang, H., and Peng, X. (2013). Laminar MoS$_2$ membranes for molecule separation. Chem. Commun. 49, 10718–10720.

109. Deng, M., Kwac, K., Li, M., Jung, Y., and Park, H.G. (2017). Stability, molecular sieving, and ion diffusion selectivity of a lamellar membrane from two-dimensional molybdenum disulfide. Nano Lett. 17, 2342–2348.

110. Wang, Z., Tu, Q., Sim, A., Yu, J., Duan, Y., Poon, S., Liu, B., Han, Q., Urban, J.J., Sedlak, D., and Mi, B. (2020). Superselective removal of lead from water by two-dimensional MoS$_2$ nanosheets and layer-stacked membranes. Environ. Sci. Technol. 54, 12602–12611.

111. Li, H., Ko, T.-J., Lee, M., Chung, H.-S., Han, S.S., Oh, K.H., Sadmani, A., Kang, H., and Jung, Y. (2019). Experimental realization of few layer two-dimensional MoS$_2$ membranes of near atomic thickness for high efficiency water desalination. Nano Lett. 19, 5194–5204.

112. Cui, X., Wu, X., Zhang, J., Wang, J., Zhang, H., Du, F., Qu, L., Cao, X., and Zhang, P. (2019). A loosely stacked lamellar membrane of irregular MoS$_2$ flakes for ultrahigh water and organics permeation. J. Mater. Chem. 7, 12698–12705.

113. Lu, X., Gabinet, U.R., Ritt, C.L., Feng, X., Deshmukh, A., Kawabata, K., Kaneda, M., Hashmi, S.M., Osuji, C.O., and Elimelech, M. (2020). Relating selectivity and separation performance of lamellar two-dimensional molybdenum disulfide (MoS$_2$) membranes to nanosheet stacking behavior. Environ. Sci. Technol. 54, 9640–9651.

114. Sun, L., Ying, Y., Huang, H., Song, Z., Mao, Y., Xu, Z., and Peng, X. (2014). Ultrafast molecule separation through layered WS$_2$ nanosheet membranes. ACS Nano 8, 6304–6311.

115. Su, Y., Liu, D., Yang, G., Han, Q., Qian, Y., Liu, Y., Wang, L., Razal, J.M., and Lei, W. (2020). Transition metal dichalcogenide (TMD) membranes with ultrasmall nanosheets for ultrafast molecule separation. ACS Appl. Mater. Interfaces 12, 45453–45459.

116. Han, J.J., Zhang, Q.Y., Huang, M.Y., Chen, Y., Yan, X., and Lang, W.Z. (2020). Two-dimensional WS$_2$ membranes constructed on different substrates for efficient dye desalination. Desalination 480, 114380.

117. Liu, L., Qu, S., Yang, Z., and Chen, Y. (2020). Fractionation of dye/NaCl mixtures using loose nanofiltration membranes based on the incorporation of WS$_2$ in self-assembled layer-by-layer polymeric electrolytes. Ind. Eng. Chem. Res. 59, 18160–18169.

118. Ries, L., Petit, E., Michel, T., Diogo, C.C., Gervais, C., Salameh, C., Bechelany, M., Balme, S., Miele, P., Onofrio, N., and Voiry, D. (2019). Enhanced sieving from exfoliated MoS$_2$ membranes via covalent functionalization. Nat. Mater. 18, 1112–1117.

119. Hu, W., Cui, X., Xiang, L., Gong, L., Zhang, L., Gao, M., Wang, W., Zhang, J., Liu, F., Yan, B., and Zeng, H. (2020). Tannic acid modified MoS$_2$ nanosheet membranes with superior water flux and ion/dye rejection. J. Colloid Interface Sci. 560, 177–185.

120. Zhang, H., Gong, X.Y., Li, W.X., Ma, X.H., Tang, C.Y., and Xu, Z.L. (2020). Thin-film nanocomposite membranes containing tannic acid-Fe^{3+} modified MoS$_2$ nanosheets with enhanced nanofiltration performance. J. Membr. Sci. 616, 118605.

121. Ma, M.Q., Zhang, C., Zhu, C.Y., Huang, S., Yang, J., and Xu, Z.K. (2019). Nanocomposite membranes embedded with functionalized MoS$_2$ nanosheets for enhanced interfacial compatibility and nanofiltration performance. J. Membr. Sci. 591, 117316.

122. Zhang, H., Taymazov, D., Li, M.P., Huang, Z.H., Liu, W.L., Zhang, X., Ma, X.H., and Xu, Z.L. (2019). Construction of MoS$_2$ composite membranes on ceramic hollow fibers for efficient water desalination. J. Membr. Sci. 592, 117369.

123. Ma, J., Tang, X., He, Y., Fan, Y., Chen, J., and Yu, H. (2020). Robust stable MoS$_2$/GO filtration membrane for effective removal of dyes and salts from water with enhanced permeability. Desalination 480, 114328.

124. Tham, H.M., Japip, S., and Chung, T.S. (2019). WS$_2$ deposition on cross-linked polyacrylonitrile with synergistic transformation to yield organic solvent nanofiltration membranes. J. Membr. Sci. 588, 117219.

125. Sreeramareddygari, M., Mannekote Shivanna, J., Somasundrum, M., Soontarapa, K., and Surareungchai, W. (2021). Polythiocyanuric acid-functionalized MoS$_2$ nanosheet-based high flux membranes for removal of toxic heavy metal ions and Congo red. Chem. Eng. J. 425, 130592.

126. Zhao, F., Peydayesh, M., Ying, Y., Mezzenga, R., and Ping, J. (2020). Transition metal dichalcogenide-silk nanofibril membrane for one-step water purification and precious metal recovery. ACS Appl. Mater. Interfaces 12, 24521–24530.

127. Yin, J., Yang, Z., Tang, C.Y., and Deng, B. (2020). Probing the contributions of interior and exterior channels of nanofillers toward the enhanced separation performance of a thin-film nanocomposite reverse osmosis membrane. Environ. Sci. Technol. Lett. 7, 766–772.

128. Tan, C., Luo, Z., Chaturvedi, A., Cai, Y., Du, Y., Gong, Y., Huang, Y., Lai, Z., Zhang, X., Zheng, L., et al. (2018). Preparation of high-percentage 1T-phase transition metal dichalcogenide nanodots for electrochemical hydrogen evolution. Adv. Mater. 30, 1705509.

129. He, Y., Tang, P., Hu, Z., He, Q., Zhu, C., Wang, L., Zeng, Q., Golani, P., Gao, G., Fu, W., et al. (2020). Engineering grain boundaries at the 2D limit for the hydrogen evolution reaction. Nat. Commun. 11, 57.

130. Li, W.X., Yang, Z., Liu, W.L., Huang, Z.H., Zhang, H., Li, M.P., et al. (2021). Polyamide reverse osmosis membranes containing 1D nanochannels for enhanced water purification. J. Membr. Sci. 618, 118681.

131. Voiry, D., Goswami, A., Kappera, R., e Silva, C.d.C.C., Kaplan, D., Fujita, T., Chen, M., Asefa, T., and Chhowalla, M. (2015). Covalent functionalization of monolayered transition metal dichalcogenides by phase engineering. Nat. Chem. 7, 45–49.

132. Hoenig, E., Strong, S.E., Wang, M., Radhakrishnan, J.M., Zaluzec, N.J., Skinner, J.L., and Liu, C. (2020). Controlling the structure of MoS$_2$ membranes via covalent functionalization with molecular spacers. Nano Lett. 20, 7844–7851.

133. Gao, J., Zhang, M., Wang, J., Liu, G., Liu, H., and Jiang, Y. (2019). Bioinspired modification of layer-stacked molybdenum disulfide (MoS$_2$) membranes for enhanced nanofiltration performance. ACS Omega 4, 4012–4022.

134. Lin, Z., Liu, Y., Halim, U., Ding, M., Liu, Y., Wang, Y., Jia, C., Chen, P., Duan, X., Wang, C., et al. (2018). Solution-processable 2D semiconductors for high-performance large-area electronics. Nature 562, 254–258.

135. Wang, C., He, Q., Halim, U., Liu, Y., Zhu, E., Lin, Z., Xiao, H., Duan, X., Feng, Z., Cheng, R., et al. (2018). Monolayer atomic crystal molecular superlattices. Nature 555, 231–236.

136. Zhou, L., He, B., Yang, Y., and He, Y. (2014). Facile approach to surface functionalized MoS$_2$ nanosheets. RSC Adv. 4, 32570.

137. Chou, S.S., De, M., Kim, J., Byun, S., Dykstra, C., Yu, J., Huang, J., and Dravid, V.P. (2013). Ligand conjugation of chemically exfoliated MoS$_2$. J. Am. Chem. Soc. 135, 4584–4587.

138. Li, Y., Liang, Y., Robles Hernandez, F.C., Deog Yoo, H., An, Q., and Yao, Y. (2015). Enhancing sodium-ion battery performance with interlayer-expanded MoS$_2$-PEO nanocomposites. Nano Energy 15, 453–461.

139. Sattari, S., Beyranvand, S., Soleimani, K., Rossoli, K., Salahi, P., Donskyi, I.S., Shams, A., Unger, W.E.S., Yari, A., Farjanikish, G., et al. (2020). Boronic acid-functionalized two-dimensional MoS_2 at biointerfaces. Langmuir *36*, 6706–6715.

140. Chen, H., Liu, B., Yang, Q., Wang, S., Liu, W., Zheng, X., Liu, Z., Liu, L., and Xiong, C. (2017). Facile one-step exfoliation of large-size 2D materials via simply shearing in triethanolamine. Mater. Lett. *199*, 124–127.

141. Chu, C., Fu, C.F., Zhang, P., Pan, T., Ai, X., Wu, Y., Cui, P., Huang, Q., and Ran, J. (2020). Precise ångström controlling the interlayer channel of MoS_2 membranes by cation intercalation. J. Membr. Sci. *615*, 118520.

142. Azamat, J., Khataee, A., and Sadikoglu, F. (2018). Computational study on the efficiency of MoS_2 membrane for removing arsenic from contaminated water. J. Mol. Liq. *249*, 110–116.

143. Masih Das, P., Thiruraman, J.P., Chou, Y.C., Danda, G., and Drndić, M. (2019). Centimeter-scale nanoporous 2D membranes and Ion transport: porous MoS_2 monolayers in a few-layer matrix. Nano Lett. *19*, 392–399.

144. Waduge, P., Bilgin, I., Larkin, J., Henley, R.Y., Goodfellow, K., Graham, A.C., Bell, D.C., Vamivakas, N., Kar, S., and Wanunu, M. (2015). Direct and scalable deposition of atomically thin low-noise MoS_2 membranes on apertures. ACS Nano *9*, 7352–7359.

145. Shen, J.-W., Li, J., Liu, F., Zhang, L., Liang, L., Wang, H., and Wu, J.-Y. (2020). A molecular dynamics study on water desalination using single-layer $MoSe_2$ nanopore. J. Membr. Sci. *595*, 117611.

146. Heiranian, M., Farimani, A.B., and Aluru, N.R. (2015). Water desalination with a single-layer MoS_2 nanopore. Nat. Commun. *6*, 8616.

147. Liu, C., Jin, Y., and Li, Z. (2019). Water transport through graphene and MoS_2 nanopores. J. Appl. Phys. *126*, 024901.

148. Yang, K., Liu, D., Qian, Z., Jiang, D., and Wang, R. (2021). Computational auxiliary for the progress of sodium-ion solid-state electrolytes. ACS Nano *15*, 17232–17246.

149. Kou, J., Yao, J., Wu, L., Zhou, X., Lu, H., Wu, F., and Fan, J. (2016). Nanoporous two-dimensional MoS_2 membranes for fast saline solution purification. Phys. Chem. Chem. Phys. *18*, 22210–22216.

150. Li, W., Yang, Y., Weber, J.K., Zhang, G., and Zhou, R. (2016). Tunable, strain-controlled nanoporous MoS_2 filter for water desalination. ACS Nano *10*, 1829–1835.

151. Cao, Z., Liu, V., and Barati Farimani, A. (2020). Why is single-layer MoS_2 a more energy efficient membrane for water desalination? ACS Energy Lett. *5*, 2217–2222.

152. Wu, K., Chen, Z., Li, J., Xu, J., Wang, K., Li, R., Wang, S., and Dong, X. (2019). Ultrahigh water flow enhancement by optimizing nanopore chemistry and geometry. Langmuir *35*, 8867–8873.

153. Abal, J.P.K., Bordin, J.R., and Barbosa, M.C. (2020). Salt parameterization can drastically affect the results from classical atomistic simulations of water desalination by MoS_2 nanopores. Phys. Chem. Chem. Phys. *22*, 11053–11061.

154. Tang, Q., and Jiang, D.E. (2015). Stabilization and band-gap tuning of the 1T-MoS_2 monolayer by covalent functionalization. Chem. Mater. *27*, 3743–3748.

155. Kwac, K., Kim, I., Pascal, T.A., Goddard, W.A., Park, H.G., and Jung, Y. (2017). Multilayer two-dimensional water structure confined in MoS_2. J. Phys. Chem. C *121*, 16021–16028.

156. Oviroh, P.O., Jen, T.C., Ren, J., Mohlala, L.M., Warmbier, R., and Karimzadeh, S. (2021). Nanoporous MoS_2 membrane for water desalination: a molecular dynamics study. Langmuir *37*, 7127–7137.

157. Ritt, C.L., Werber, J.R., Deshmukh, A., and Elimelech, M. (2019). Monte Carlo simulations of framework defects in layered two-dimensional nanomaterial desalination membranes: implications for permeability and selectivity. Environ. Sci. Technol. *53*, 6214–6224.